Development of a Cryogenic EBID Method for Fabricating Nanowires using a W(CO)6 Precursor

Sohl, Bernard

Development of a Cryogenic EBID Method for Fabricating Nanowires using a $W(CO)_6$ Precursor

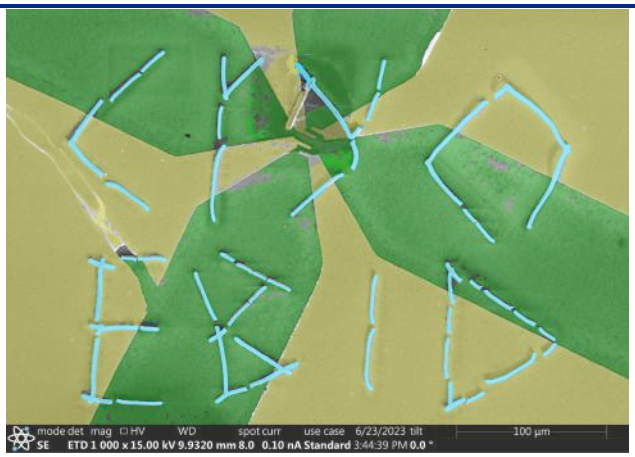

THESIS

submitted in partial fulfillment of the
requirements for the degree of

BACHELOR OF SCIENCE
in
PHYSICS

Author :	Bernard Sohl
Student ID :	2598914
Supervisor :	Dr. Kaveh Lahabi
Second corrector :	Dr. Semonti Bhattarachyya

Leiden, The Netherlands, June 28, 2023

Development of a Cryogenic EBID Method for Fabricating Nanowires using a $W(CO)_6$ Precursor

Bernard Sohl

Huygens-Kamerlingh Onnes Laboratory, Leiden University
P.O. Box 9500, 2300 RA Leiden, The Netherlands

June 28, 2023

Abstract

This thesis presents a detailed study into the development of a custom-made cryogenic sample stage which was designed, fabricated, and retrofitted in a Scanning Electron Microscope (SEM) for performing Cryo-EBID, a cryogenic variation of the microfabrication technique known as 'Electron Beam Induced Deposition' (EBID). It provides an overview of all relevant aspects of the design process, from the concept design to a fully integrated and functional product. The goal of the project is to implement Cryo-EBID for the fabrication of nanowires using a tungsten hexacarbonyl ($W(CO)_6$) precursor, offering an immense increase in deposition rate compared to traditional EBID. The setup's efficacy in creating microstructures is evaluated at various electron doses and a small set of prototype nanowires were fabricated and characterized. This project serves to provide valuable insights into the development process of a cryogenic sample stage and a method for creating nanowires using cryo-EBID while also setting the stage for future cryo-EBID experiments.

Contents

Chapter 1

Introduction

Electron-Beam-Induced Deposition (EBID) is a single-step technique to create freestanding 3D structures at the sub-10 nm scale by focusing electron beams at gaseous precursor molecules leading to deposition onto a substrate. This effect has been known since 1934 when deposits of organic material were found in electron and ion bombardment experiments. [18] The deposition occurs because of the interactions between the electrons and the precursor gas, causing the molecules to dissociate into multiple volatile and non-volatile components, the latter of which the latter interacts with the substrate and forms a deposit. Three things are essential when performing EBID: a good vacuum, a focused electron beam, and a precursor gas.

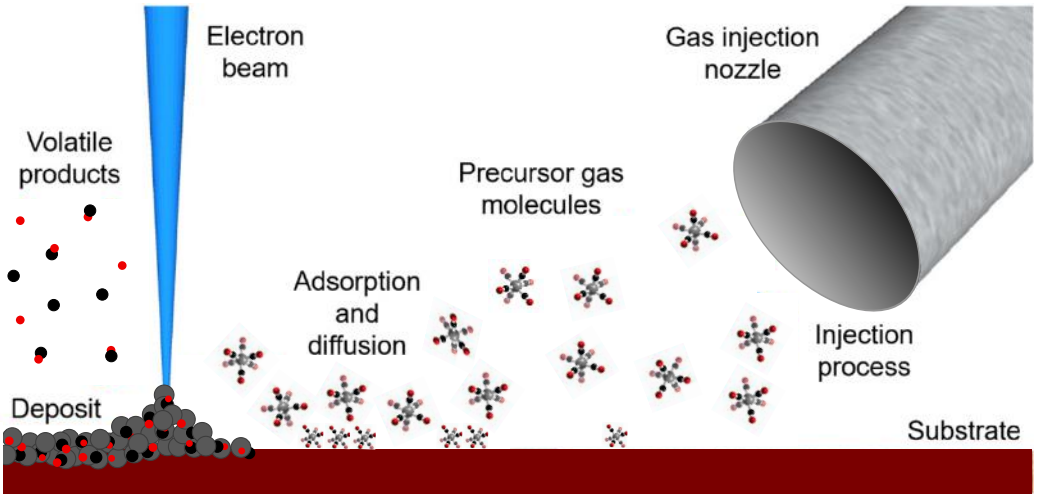

Figure 1.1: *Diagram Displaying the EBID process*

Luckily, there is equipment readily available which is capable of all three: Scanning Electron Microscopes (SEM). To perform EBID, an SEM is equipped with a Gas Injection System (GIS) for precise delivery of the precursor gas. [16]

EBID is an often overlooked technology in the field of micro-fabrication and has to compete with more traditional methods such as Electron Beam Lithography (EBL) and photolithography. In contrast, EBID is known as a 'Direct-write' method of lithography where a pattern can be directly written onto a substrate. The other methods of lithography employ a so-called 'mask' or 'stamp' to transfer a pattern onto a substrate. The advantage of EBID is that it is exceptionally versatile as there are no steps between designing a pattern and writing, it also negates the need for masks, expensive clean rooms, or extensive training, which is all essential for the more traditional methods of microfabrication. EBID is remarkably suitable for many applications including repairing of photomasks [8], direct fabrication of nanowires [17], and superconducting quantum interference devices (SQUIDs) [4]. The downside of EBID is that is unsuitable for mass production. Every element of the pattern has to be traced over with EBID whilst it is possible to provide a mask with multiple copies of a pattern which can all be written at once.

The goal of this project is to create a method utilizing EBID to create nanowires for creating contacts for a currently ongoing project of a SQUID-on-tip, where nano-SQUID magnetometers are created on the tip of a scanning probe to study magnetic and thermal phenomena with amazing spatial resolution. Unfortunately, creating contacts to these SQUIDs

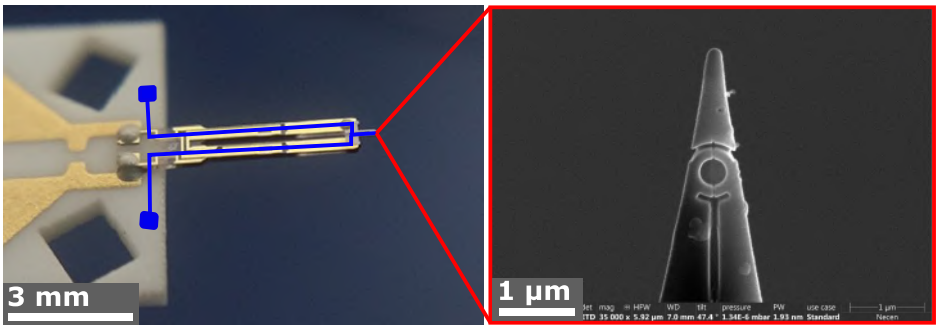

Figure 1.2: *(Left): NANOSENSORS™Akiyama-Probe. (Blue): area requiring a conductive path to be deposited. (Right): A SQUID manufactured on the tip of the Akiyama-Probe. Image Courtesy of M. Rog.*

has proven to be a tedious challenge. These contacts were made using the multi-step process of employing a hard mask and etching away excess material using a focused ion beam (FIB), which could easily take upwards of days. Using EBID for contacting the SQUIDs has been considered as a solution for this problem as one could just deposit wires from the SQUID to the contact points but was unfortunately proven not fit for the job as the deposition rate using traditional EBID is insufficient. With the lateral deposition rate of EBID only being on the order of 20 nm/s [12], creating nanowires on the order of millimeters would be impractically time-consuming.

Chapter 2

Cryo-EBID

A possible solution to this slow deposition is the utilization of cryo-EBID, where you perform EBID at cryogenic temperatures by cooling down the substrate. The deposition rate using EBID can be limited by two extremes: the electron-limited regime, where there are insufficient electrons to dissociate the precursor molecules, and the precursor-limited regime, where the precursor molecules cannot get replenished quickly enough at the deposition site. In the case of depositing nanowires, the deposition predominantly falls into the precursor-limited regime. This lack of available precursor molecules can be omitted by cooling down the deposition substrate such that the precursor forms a condensate layer on the substrate instead of relying on the precursor molecules to momentarily be adsorbed to the substrate surface. This layer ensures the presence of precursor molecules on the deposition site, effectively eliminating the precursor-limited regime. Using cryo-EBID has been shown to increase the deposition rate up to four orders of magnitude versus room temperature EBID (RT EBID) [5]. When performing cryo-EBID, the GIS is opened for a certain amount of time to create a film of condensate precursor material, the electron beam will write a pattern on the condensate after which the substrate is heated up again, desorbing the condensate which has not been dissociated. The following sections will revolve around the most important aspects which come about when performing EBID on cryogenic temperatures.

Precursor

One of the most important factors in the EBID process is the choice of precursor. An EBID precursor is typically metallo-organic, which is a class

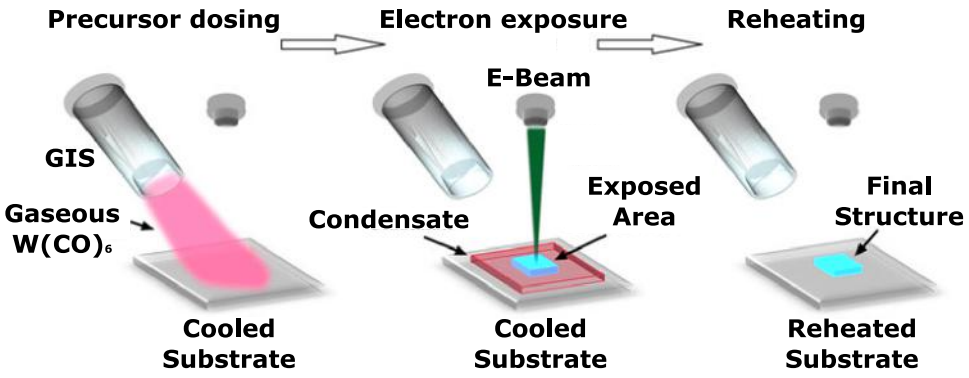

Figure 2.1: *Diagram displaying the Cryo-EBID procedure.*

of molecules consisting of metals and organic ligands. The resulting deposits of these metallo-organic compounds are a mixture of a metal and the elements contained in the organic ligands. Next to the metallo-organic precursors, there is also a class of organic precursors, used for creating deposits containing mainly carbon. These will not be suitable for this project due to poor conductive properties [6].

Tungsten Hexacarbonyl [W(CO)6]

The available precursors for the project are tungsten hexacarbonyl [$W(CO)_6$] and Trimethyl(methylcyclopentadienyl)platinum(IV) (MeCpPtMe3), which can be used to deposit W-C and Pt-C structures respectively. The tungsten hexacarbonyl precursor was eventually chosen as the W-C deposits exhibit a higher metal content and better conductivity values. For reference, performing EBID with an electron energy of 1 kV, the W-C deposit contains 20% W whereas the Pt deposit only contains 10% Pt [7]. W-C deposits have even been shown to be able to become superconducting when a sufficient atomic percentage of tungsten is present in the deposit, starting at between 28% and 34% [4].

Beam Parameters

Next to the precursor, the parameters of the electron beam are crucial to controlling the outcome of the deposit. The effective amount of electrons in the electron beam can be described with the current density [A/cm^2] which is dependent on the beam current, often given in units of picoamperes (pA), spot size which determines the effective area of the electron

beam and dwell time, which is the time for which the electron beam irradiates each spot. The current density is mostly responsible for the effective growth rate, more electrons mean that more precursor molecules can be disassociated and thus deposited. With a constant gas flux and spot size, a higher current density results in a higher growth rate. The increase in growth rate diminishes with a growing current density as the system meets the precursor-limited regime [12]. The current density also increases the metal content in the deposition. When the system reaches the precursor-limited regime, there is a higher chance for the precursor molecules to get hit by the electrons which increases the number of ligands which can dissociate, increasing the concentration of metal in the final deposit and is beneficial for the metallic properties [19].

Substrate temperature

The most important parameter in the cryo-EBID process is the substrate temperature, as it enables an increase in the writing speed of several orders of magnitude. Changing the substrate temperature induces several changes in the parameters of the EBID process. As mentioned before, cooling down the substrate causes the precursor molecules to desorb at a slower rate or even form a condensate layer, eliminating the precursor-limited regime. Changing the temperature of the substrate also seems to affect the purity of the deposits depending on the precursor. Using a $W(CO)_6$ precursor, the atomic percentage of W has been shown to increase from approximately 35% to about 55% when heating from room temperature to 300°C [13]. The extra thermal energy facilitates the dissociation of organic ligands, thus decreasing the quantity of organic material in the final deposit. Therefore, altering the substrate temperature represents a trade-off between deposition rate and deposition purity.

Version of June 28, 2023– Created June 28, 2023 - 15:33

Chapter 3

Materials and methods

We will tune the parameters of the EBID process to our advantage and attain deposition rate orders of magnitudes higher than traditional RT EBID. The parameters to adjust concerning RT $W(CO)_6$ EBID are the beam parameters and the substrate temperature. The EBID is performed in a Thermofisher Apreo 2 SEM, which has configurable beam parameters, it does however lack the ability to change the substrate temperature in its current state. Therefore, a custom solution was, with the help of the university's Fine Mechanics Department (FMD), designed, manufactured and integrated into the Apreo 2 SEM. In the following section, we will go over all the factors which were involved throughout the whole process, from the initial stages to the finished product.

3.1 Problem Overview and Considerations

All options for cooling down a sample in the Apreo 2 SEM were explored. The first and most obvious option was to acquire a cryogenic sample stage. Unfortunately, this would exceed the scope of the project due to a limited budget and time frame. The second option was to make use of the Thermofisher Aquilos cryo-FIB from the Netherlands Centre for Electron Nanoscopy (NeCEN), which is an independent facility located at the Institute Biology Leiden (IBL) at Leiden University. The Aquilos cryo-FIB can do the same as the Apreo 2 SEM but with the added benefit that it is fitted with the additional Thermofisher cryostage. However, this option did not provide the required flexibility of use for the project as we do not want to rely on a third party to perform cryo-EBID. The most fitting solution would be to design and fabricate my cryostage and have it retrofitted into

the Apreo 2 SEM. The cryostage was designed taking into account various criteria, the following sections will provide a comprehensive overview of these criteria.

Compatibility and versatility

First and foremost, the cryostage needs to be compatible and integrable in the Apreo 2 SEM without interfering with other people's research as the SEM is a shared instrument among the LION members. To control the temperature of a sample in the sample chamber, we need a vacuum-compatible thermal feedthrough to extract heat from the sample and an electrical feedthrough to read out a temperature sensor and power a heating element for heating the sample back up to room temperature. The SEM was not equipped with a thermal feed-through so we had to construct a custom design that would fit on the only available vacuum port which was covered by a large blank flange seen in Figure 3.1(a). The SEM is fitted with a three-way hub containing three electrical ports of the C-type subminiature, a common type of electrical connector used in vacuum systems.

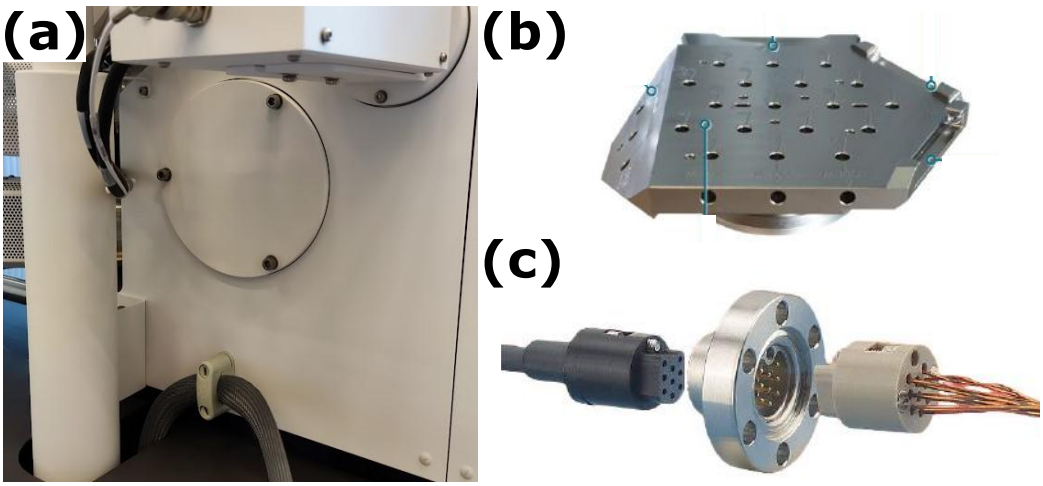

Figure 3.1: *(a): The blank flange positioned on the left side of the chamber, (b): the SEM sample stage. Image source: Thermofisher. (c): A sub-C type 9-pin electrical feedthrough. Image source: [ele],*

So only the cables for both the air and vacuum side had to be acquired to create an electrical connection. At last, the cryostage needed to be com-

patible with the sample holder of the SEM, it should be able to be attached to the sample stage to retain the ability to move the sample. To keep the setup from hindering other people's research, the setup needs the capability to be set up and removed in one session. The setup should therefore be versatile and easily detachable from the SEM. To achieve the desired versatility, it was necessary to avoid unnecessary complexities and keep the setup as simple as possible.

Thermal performance and insulation

Another integral part of the design would be to ensure that the sample could cool down sufficiently to temperatures below -50 °C at an acceptable rate. There were three approaches to this problem: the first method utilizes a liquid feedthrough to feed liquid nitrogen through a cold finger to the stage [11], the second is to use an array of thermometric plates and uses a liquid feedthrough to feed cooling water to the stage to transfer the heat of the hot side of the array [14], and the third method is to use a solid thermal feedthrough and cold finger made entirely of copper which is cooled down from the outside to cool down the stage [2]. The first and second option seems to be the fastest as they would deliver instant substantial cooling power as they involved a moving medium to transfer thermal energy from the stage. Using solid copper for the feedthrough and cold finger would rely on thermal diffusion to cool down a sample, which is less conductive with orders of magnitude. The disadvantage of using a liquid feedthrough is that such a system would require firm feedthrough tubes in the inside of the SEM which would prevent the stage from being able to move, these tubes would also not be able to be removed easily and would also require large equipment such as watercoolers or a liquid nitrogen reservoir which would make the process overly complicated. The only method which would fit into the scope of this project was to use a solid copper feedthrough and a flexible copper braid as a cold finger such that the sample stage would still be able to move with the cryostage. To provide the versatility of the setup, the cold finger would have to be detachable from the flange, allowing the entire setup to be moved inside and outside the chamber easily.

In addition, it is important to ensure the system was thermally but not electrically insulated from the SEM. The thermal insulation is crucial, parts of SEM could leak heat into the system, impairing the thermal performance of the stage. Poor thermal insulation would also mean that parts of the SEM will be subjected to really cold temperatures which they were

not designed for, possibly damaging parts of the SEM or impeding normal function. The cryostage does have to be electrically connected to the SEM to unload the electrons brought in by the electron beam, the lack of proper grounding would give rise to charging of the sample, leading to uneven brightness, bright stripes and distortions in the SEM image.

Reliability and safety

Safety and reliability are crucial to the cryo-EBID process. Ensuring the safety of the user involves preventing exposure to cryogenic temperatures without the proper safety equipment, cold surfaces should also be shielded or insulated to prevent accidental contact. When using an SEM, beta and X-ray radiation is emitted, therefore it is important that the thermal feedthrough is impermeable to these forms of radiation while retaining enough structural rigidity to prevent an implosion of the sample chamber. The setup should be sturdy and able to withstand large temperature fluctuations to ensure long-term usability.

The cryo-EBID process should also be reliable and repeatable. The setup should be user-friendly such that experiments can be easily repeated and give consistent results. Furthermore, it is important to maintain consistent vacuum pressures in the sample chamber, also after cryo-EBID ex-

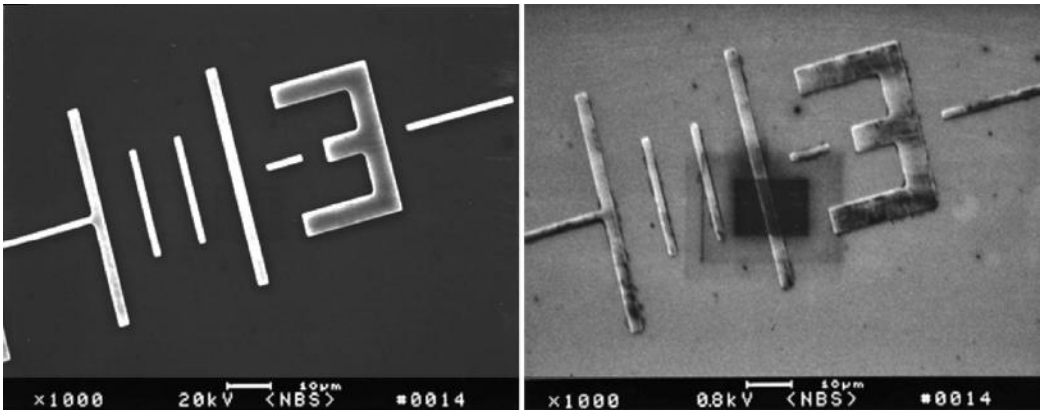

Figure 3.2: *Typical example of contamination deposits on a patterned silicon wafer. The rectangular shape is due to the shape of the viewing box when looking at a sample in live mode. (Left): High electron energy (20 keV) image of the contaminated area. (Right): Low electron energy (0.8 keV) image of the contaminated area, the contamination is more visible to lower energy electrons due to the lower penetration depth and thus a higher degree of interaction. Image Source: [15]*

periments. To ensure this, we should be wary of contaminants that could outgas at vacuum pressures and contaminate the vacuum. Outgassing could occur in contaminants such as oils from the skin or fabrication process or materials used in the setup such as plastics or organic materials. Keeping the setup clean also prevents the contamination of the sample stage of the sample chamber which could interfere with other people's experiments. These contaminants also affect the cryo-EBID process by compromising the quality and integrity of the deposits. The outgassing of the contaminants could cause them to enter the precursor condensate and therefore reducing the quality of the deposit. Moreover, the contaminants could be inadvertently deposited due to the electron beam, or adhere to the cooled substrate prior to releasing the precursor on the condensate. The deposit near the substrate surface would therefore be more contaminated, compromising the surface adhesion of the deposit.

The setup should also be free of so-called 'virtual leaks' which are trapped volumes of gas that could slowly leak into the vacuum chamber, resembling a leak as the chamber will not be able to reach sufficient vacuum pressures due to the constant flow of gas. These gas volumes are usually located at the end of a tapped hole, behind a fastener, which will slowly escape through the screw thread. This can be negated by using vented screws, which are screws with a venting hole leading to these voids, allowing the gas to escape quickly

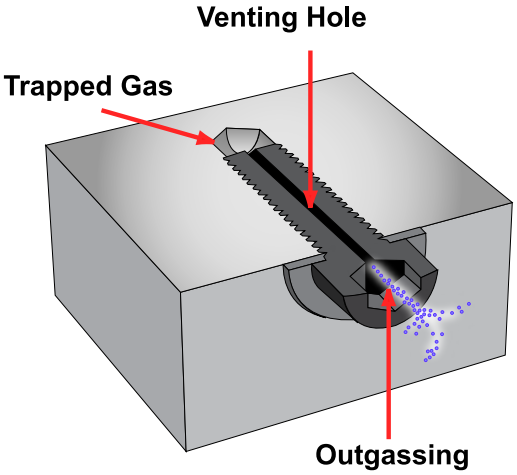

Figure 3.3: *A vented screw.*

3.2 Design process

A cryogenic sample stage would be placed on the SEM sample stage which was connected to a flexible copper braid that served as a cold finger. This cold finger would be connected to a thermal feedthrough passing through a vacuum flange which would be cooled down using liquid nitrogen on the air side. Liquid nitrogen was chosen because of its ease of use and enormous cooling capability. The design consisted of two main components: the cryostage and the thermal feedthrough. The design process started with the cryostage, followed by designing the thermal feedthrough which would be compatible with the cryostage. By breaking up the design chronologically, the design process would become more systemic. All designs were done with Autodesk™Inventor which is a 3D Computer Assisted Design (CAD) program. The detailed technical drawings reside in the appendix.

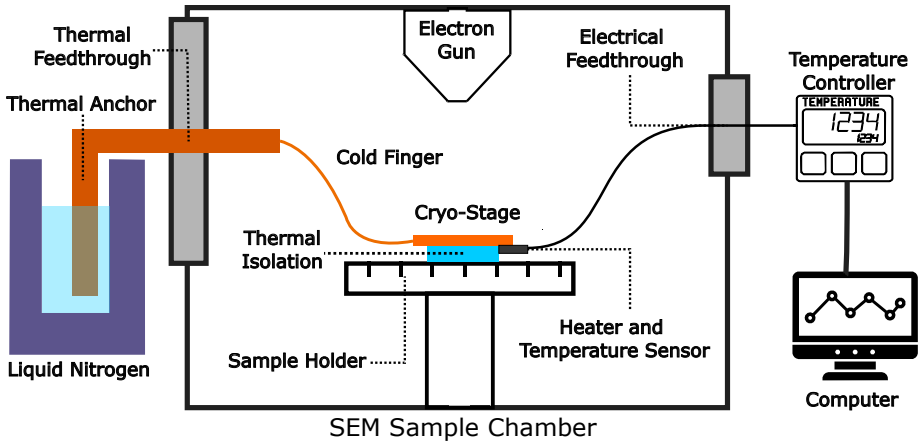

Figure 3.4: *Schematic representation illustrating the full overview of the project's structure.*

3.2.1 Cryogenic stage

Version 1.0 : The goal was clear: to create a cryogenic sample stage with a connection to a copper braid, a heating element and a temperature sensor while ensuring electrical and thermal insulation. The following section will focus on the design process and the decisions involved.

The first design took inspiration from the conventional method of placing samples on the sample stage, using an SEM stub. An SEM stub is a small sample holder which can be placed on the sample holder, it features a mushroom-shaped design with a flat metal disc on top on which a sample can be placed and a thin holding pin on the bottom side which can be put in one of the mounting holes seen in **??**. The first design would be designed after these stubs, the cryostage would be a copper puck-shaped stage attached to an insulating ceramic stub which would be placed on the sample stage. The stage would be equipped with a removable 'thermal strap' which acts as the cold finger and a PT-1000 temperature sensor. A PT-1000 temperature sensor is a Resistance Temperature Detector (RTD) consisting of a thin wire made from platinum, a PT-1000 is characterized by having a resistance of 1000 Ohms at a temperature 0°C. A PT-1000 was chosen due to its high accuracy, wide temperature range of -200°C to 150°C and a near linear relationship between resistance and temperature of approximately 4 Ohm's per Kelvin.

Figure 3.5: *SEM sample stub*

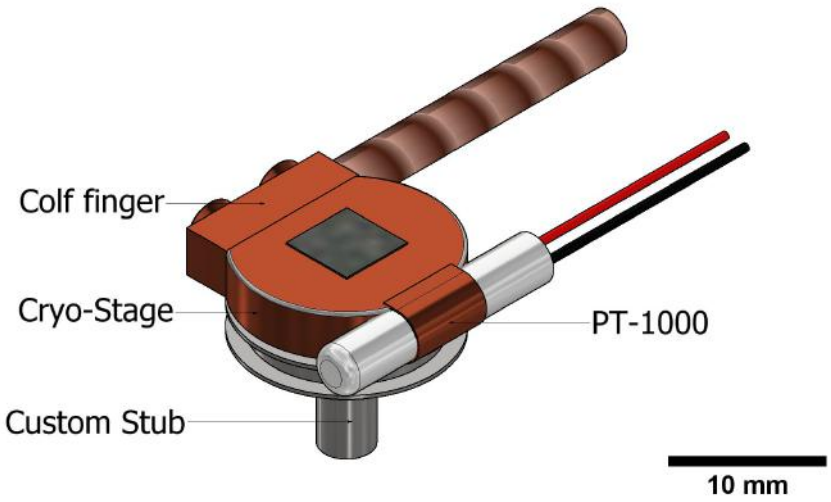

Figure 3.6: *Cryostage V1; The first finished version of the concept design of the Cryo-stage*

This design came with its advantages and disadvantages. Because the stage would be the size of a regular SEM stub, having a diameter and height of 12,7 and 3 millimeters respectively, it ensured compatibility with the sample sizes typically used. The compact size of the stage would also result in a smaller thermal mass of merely 2.6 grams, which would significantly reduce the time it would take to change the temperature of the stage. However, the small size of the stage would also be its limitation. With dimensions no larger than a standard die, it would be too fragile to reliably work with. The stage could also only fit one sample per thermal cycle, one would need to repeat the entire thermal and vacuum cycle to swap out a sample. No thermal calculations were performed at this stage since the design only served as a concept and large changes were expected to come based on feedback.

Version 2.0 : After identifying the limitations and shortcomings of the first design, several revisions were made to various aspects of the stage. The most notable being that the stage was effectively doubled in diameter. the initial dimensions of 3mm in height and 12,7mm in diameter were replaced with a larger size of 5mm in height and a diameter of 25,4mm, now bearing a mass of 19 grams. This diameter is one of the standardized sizes for SEM stubs, allowing for larger or multiple smaller samples to be placed in the SEM. The cold finger design was also revised, the single 3mm diameter copper braid was replaced with two larger 5mm diameter copper braids. This resulted in a six-fold increase in the inner diameter and thus higher thermal transfer power of the cold finger.

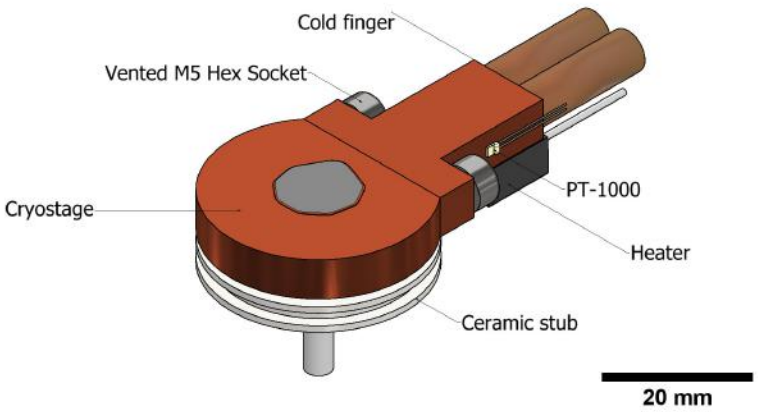

Figure 3.7: *Cryostage V2; The first revision of the initial concept design*

Furthermore, the setup also saw a revision in its electronic elements. The original wire-wound PT-1000, which involved the platinum wire being wound around a ceramic 'bobbin' to form a small cylinder, was replaced with a much smaller Thin-film Yageo Nexensos 32207502 PT-1000. Which could easily be fixed to any flat surface of the stage instead of creating a slot for the cylindrical wire-wound PT-1000 to fit in. The increased size allowed for the inclusion of a Vishay 47Ω 50W RTO050F47R00JTE1 power resistor which serves the purpose of heating the stage back up and/or baking the sample. This resistor is suitable for this design as its dimensions align well with the size of the cryostage and provides an abundance of heating power. At 50 watts, the heating power is comparable to that of an average soldering iron.

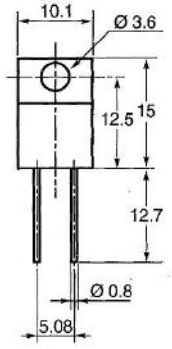

(a) *Image courtesy of Vishay™*

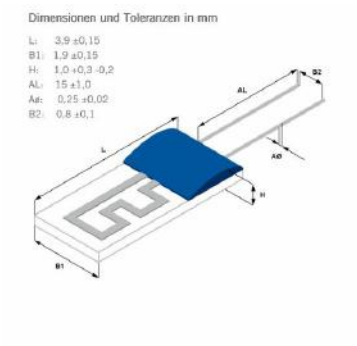

(b) *Image courtesy of Yageo nexenos™*

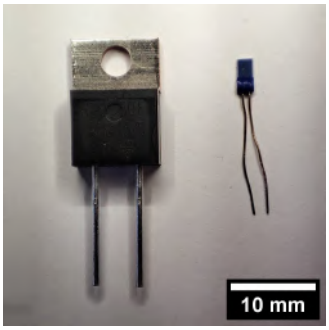

(c)

Figure 3.8: *(a): technical drawing of the Vishay 47Ω 50W RTO050F47R00JTE1 resistor, (b): technical drawing of the Yageo Nexensos 32207502 PT-1000, (c): The used components*

In the new design, the thermal insulation from the sample stage was addressed. In the first design, the stage was to be fixed to a ceramic stub using vacuum epoxy or any other kind of vacuum-compatible glue. With the new design, the increased thermal contact surface between the stage and the stub became a concern for thermal insulation. Therefore, a new method of attaching the stage to the stub was developed. The method took inspiration from that of a 'kinematic mount', a mechanical device typically used for precise alignment of optical components consisting of three or more adjustable contact points allowing for precisely controlled movement of a mounted component. The design consists of three Alumina beads placed between the stub and the stage.

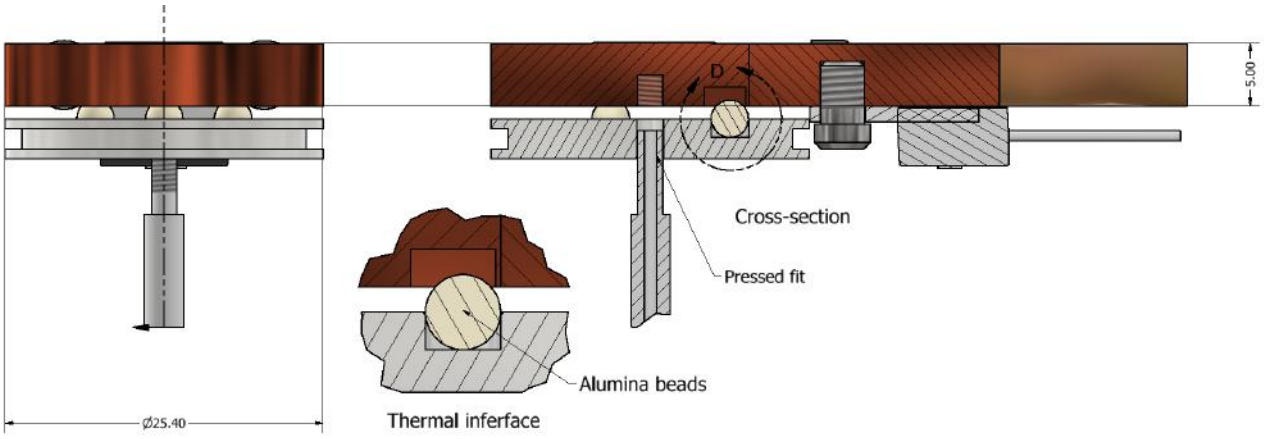

Figure 3.9: *(Left): Front View, (Middle): Section View of the thermal interface between the stage and stub, (Right): Cross-sectional view of the stage.*

Alumina is a form of aluminium oxide (Al_2O_3), known for its excellent electric insulation properties and has a thermal conductivity 16 times smaller than that of copper. The beads are held in place in the stub using three blind holes and within the stage with three wide slots to allow for thermal expansion or contraction of the stage. The stub and stage are pressed against each other with the holding pin of the stub, functioning as a thumb screw, to ensure a tight fit for the beads. This design significantly improved the thermal insulation due to alumina's poor thermal conductivity and effectively eliminated conductance between the stub and stage.

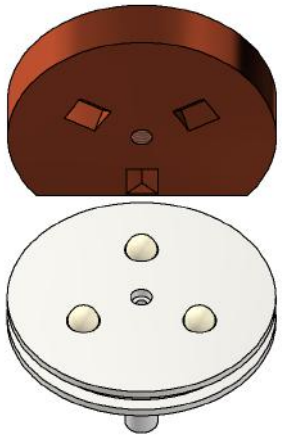

Figure 3.10: *An opened view of the interface between the stub and cryostage*

After the first revision was finalized, it was reviewed once more and feedback was given. It became evident that several aspects of this design required revision. Although the stage had been made larger, it was still not large enough. A larger stage was a practical consideration as there was more than sufficient cooling power available using liquid nitrogen, the increase in size also allowed for even more samples to be cooled down which could prove to be convenient in future use cases. Furthermore, a

more sturdy method for placing the stage on the sample stage was suggested as using a single pin may be too fragile. A single pin would also allow for the stage to rotate on its axis due to the cold finger or wires when moving the stage. While at first, this may not appear as a problem since the pin was designed to have a tight fit in the sample holder, repeated use could lead to wear and loosening of the fit.

Version 3.0 : In summary, the design required improvements in both its size and stability. The stage was once again increased in size, with the height expanding from 5mm and the diameter from 12.7mm to 10mm and 38mm, respectively. This enlargement significantly raised the mass from 19 grams to 85 grams. The increased size also brought about a shift in the design concept, as at this size, the stage resembles a cooled sample stage more than a cooled sample stub. The stage was now designed to have its own stub holes and custom copper sample stubs. The stage featured 5 holes and offered two different configurations, either using a single large 38mm diameter copper stub in the central hole or four regular-sized 12.7mm diameter copper stubs in the corner holes. This new design allowed the stage to stay on the SEM sample stage during the process of loading and unloading samples using the stubs, eliminating the need to disconnect the cold finger and electrical connection when handling samples, simplifying the process.

The method of attaching the cryostage to the sample stage was also revised significantly, replacing the relatively fragile kinematic mount with three polyetheretherketone (PEEK) stub pins featuring an enlargement on the upper side to create space between the cryostage and the sample stage.

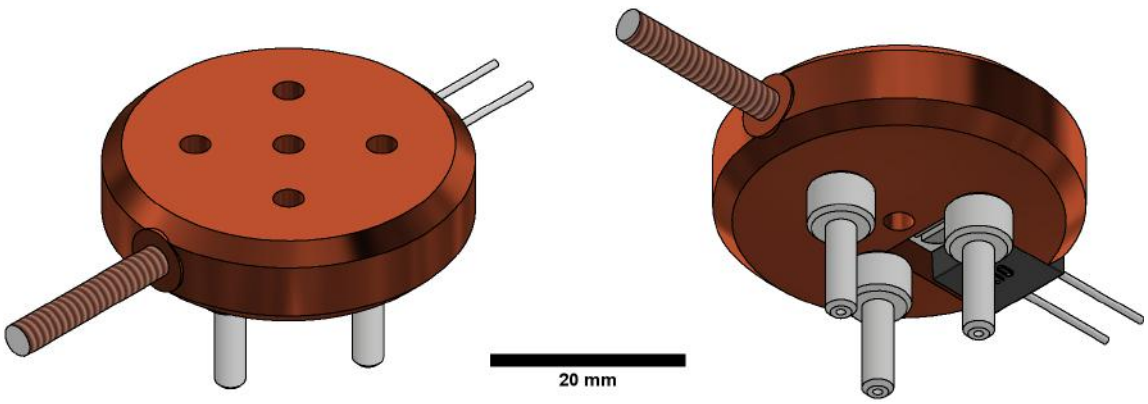

Figure 3.11: *The third and final revision of the cryostage*

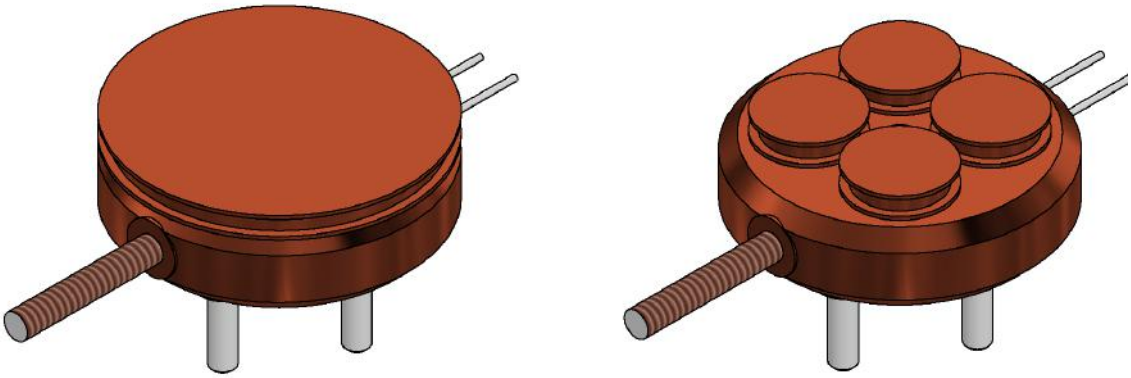

Figure 3.12: *(Left): cryostage equipped with the large 38mm stub, (Right): cryostage equipped with four 12.7mm stubs*

PEEK, a polymer plastic with excellent low-outgassing, mechanical and chemical resistance properties, features an extremely low thermal conductivity of 0.25 W/m·K compared to copper's 398 W/m·K. The bottom of the stage contains three tapped holes in which three vented grub screws are screwed that stick out, the top of the feet also contains a tapped hole and a thinner vent hole such that the feet can be screwed onto the grub screws. This method allows for sturdy attachment and easy repair or replacement when necessary and prevents outgassing due to a venting duct from the bottom of the feet to the bottom of the tapped hole. refer to 3.14 for an illustration.

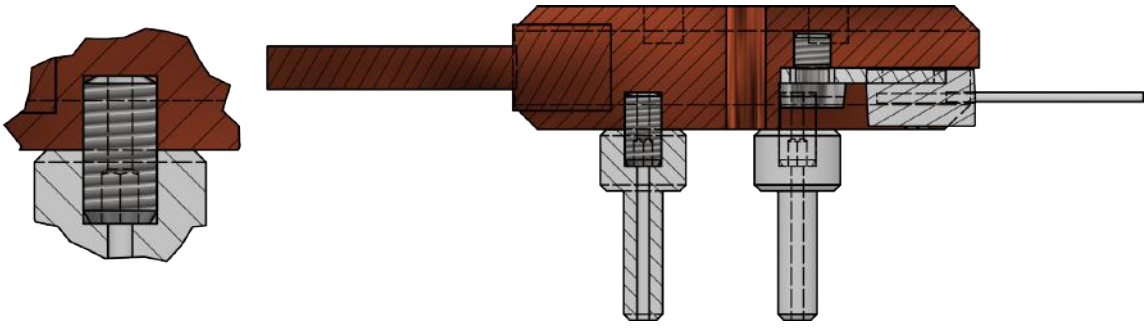

Figure 3.13: *(Left): A section-View of the method of securing the PEEK feet to the stage. (Right): Cross-sectional view of the third and final revision of the cryostage*

It is worth noting that throughout the design process, our research group and the FMD were both actively consulted during a series of sessions to ensure the stage met the specific requirements for cryo-EBID and

that the stage aligned with the manufacturing capabilities of the FMD. During these sessions, our goal was to find a balance between EBID performance and ease of fabrication. As a result of these sessions, the final design was developed and ultimately chosen for fabrication.

3.2.2 Cold finger

The cold finger serves the purpose of transferring thermal energy from the cryostage to the thermal feedthrough in the chamber wall. The cold finger was selected to be made out of Oxygen Free Copper (OFC) braid. OFC is copper which has gone through electrolytic refinement to reduce the amount of impurities to a trace amount of oxygen. The cold finger needed to efficiently transfer heat while maintaining its flexibility, therefore a balance between being thick enough to transfer more heat and thin enough to retain flexibility had to be found. For the cold finger, we used two and a half OFC braids with a cross-section of 6mm^2 resulting in a final inner cross-section of 15mm^2, this was done by using a single braid as the core and wrapping this in the individual strands of the other one and a half copper braid to create a single thicker copper braid. One end of the copper braid was crimped into a cylinder using an industrial-grade radial crimping press such that the copper braid merges with the cylinder to create an insert that can fit into the cryostage. The other side was crimped into a thicker cylinder which was machined to have a flat top with a hole to screw the cold finger to the thermal feedthrough.

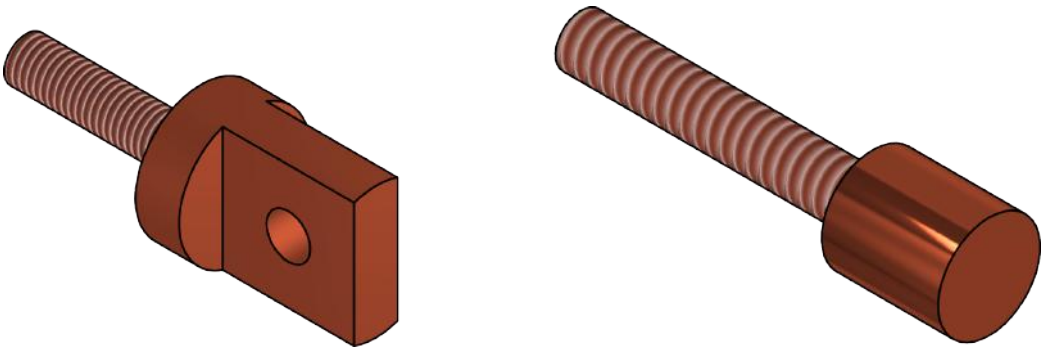

Figure 3.14: *(Left): The end of the cold finger which connects to the thermal feedthrough (Right): The end of the cold finger which is inserted into the cryostage*

It should be noted that only the center braid was crimped into the lugs and that the additional strands were wrapped around the core after that as they were added at a later moment. To fully integrate this outer layer

of copper braids, it was compressed against the inner copper braid using a steel hose clip and tightly wound copper wire. The cold finger was also insulated using a Teflon spiral wrap to prevent thermal contact between the cold finger and parts of the SEM.

(a) ***(b)***

Figure 3.15: *(a): The cold finger attached to the cryostage (b): The cryostage from a bottom-view*

We noticed that the cold finger, intended to fit tightly into the cryostage, was machined too small in diameter, resulting in a loose fit and a poor thermal connection. Therefore a tapped hole was added perpendicular to the cold finger insert hole, allowing for the insertion of a long thumb screw. By turning the screw, the cold finger would be secured tightly to the cryostage. This resulted in the thermal contact only being on a thin line on which the cold finger was pressed against the insert hole. To resolve this problem, a Thermal Interface Material (TIM) has to be used, an often viscous or malleable material that is inserted between two thermal interfaces to increase the thermal conductance. Traditional TIMs, such as hydrocarbon or silicone-based greases, were unsuitable for this application due to outgassing and creep transport properties *, which would both interfere with the cryo-EBID process. The only suitable TIM was the metal Indium, due to its high thermal conductivity and malleability, allowing the indium to fill the microscopic voids and greatly enhance thermal con-

*Creep transport refers to the movement of fluids over surfaces due to capillary action.

tact. A thin strip of indium foil was applied on the cold finger, which would spread out due to the pressure of the thumb screw. Later this indium foil was also integrated into the clamped connection between the inner copper braid and the copper strands around it to further increase the thermal conductivity.

3.2.3 Thermal feedthrough

After completing the cryostage and cold finger, our focus was aimed on designing the thermal feedthrough. The goal was to create a custom flange that accommodates a copper rod that serves as the thermal feedthrough. The rod was connected to the cold finger on the vacuum side and to a 'thermal anchor' on the air side, a component designed to be in contact with the liquid nitrogen. These thermal anchors usually consist of many thinner copper braids to maximize surface contact with the liquid nitrogen, we chose a solid copper rod as such a copper braid would also be very prone to oxidation and degradation. We also chose to make the thermal anchor have a screw-on connection to the feedthrough, allowing for replacement when needed. The thermal anchor will be positioned inside a small 1L glass dewar flask designed for handling cryogenic liquids.

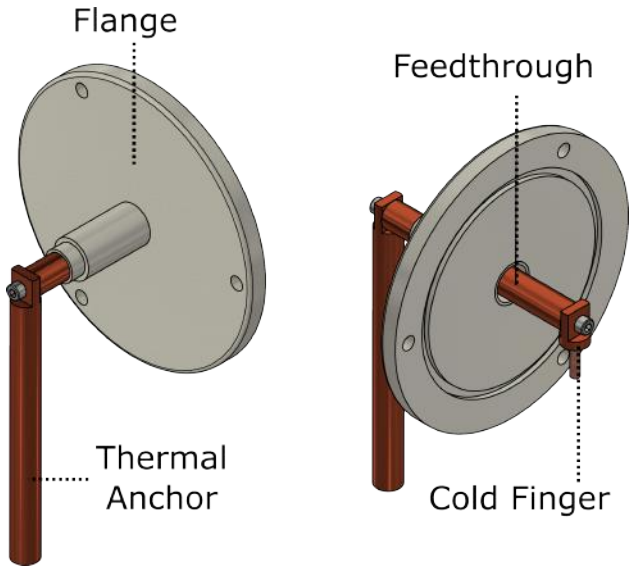

Figure 3.16: *The full thermal feedthrough design*

The SEM makes use of the ConFlat (CF) type of flanges, see figure **??**. The size of the flange that we were going to replace was not standardized

so we carefully measured the dimensions of a spare blind flange and had a copy manufactured by the FMD which would be modified to contain a thermal feedthrough. To ensure good thermal performance, it is essential to minimize the thermal transfer between the flange and copper rod while also maintaining structural rigidity and x-ray impermeability and an air-tight seal. This can be achieved by using a thermal break, which involves a low-conductivity material placed between two connected structures. Alternatively, the thermal path could also be made longer and narrower to increase thermal resistance.

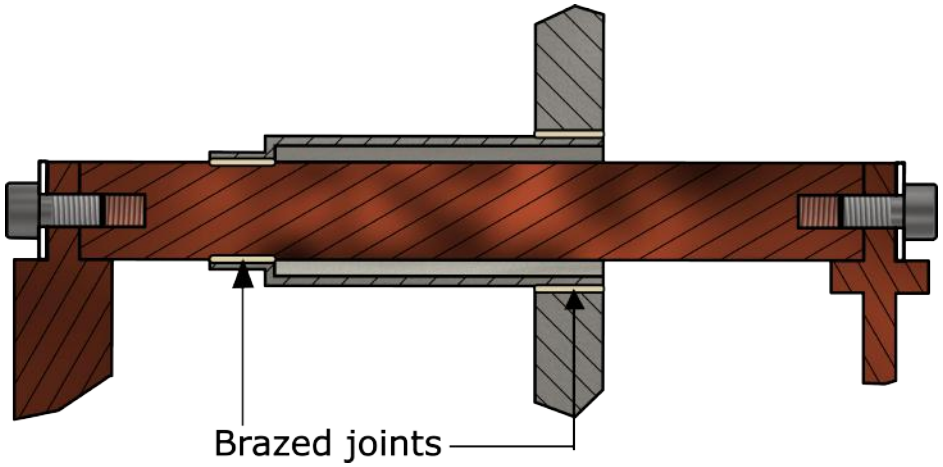

Figure 3.17: *Cross-section of the thermal feedthrough showcasing the stainless steel tube acting as the thermal resistor between the feedthrough and the flange.*

The final design of the flange opted for the second method considering it is more simple to manufacture and more reliable. Creating a vacuum-tight joint between an insulating material such as a plastic or ceramic material and metal is much more challenging than creating a joint between two metals, with 'joint' referring to a connection or joining point of two components. The design made use of a thin elongated stainless steel tube extending out of the chamber, serving as the connection between the flange and feedthrough. This tube has a larger diameter and goes around the rod, only being connected to the rod and flange on both ends. This construction only required two vacuum-tight joints, these joints were made using the process of brazing. Brazing involves melting and flowing a filler metal between the gaps of a metal-to-metal joint due to capillary action, creating a very sturdy and airtight seal. In our design, silver was used as a filler metal and brazed in the joints between the rod, pipe and flange as seen in 3.19.

To ensure that there was no large thermal transfer from the rod to the flange, thermal simulations were performed using Autodesk™Fusion360. The Inventor CAD models could easily be transferred to Fusion360 to perform a thermal study on the design. In the simulation, the thermal anchor was held at a constant temperature of -195.8C and the contact surface of the flange with the SEM chamber wall was also held at a constant room temperature of 25C. The simulation only takes into account thermal transfer with the surroundings using radiation and convection.

The results of the simulation provided valuable insights into the performance of the thermal feedthrough, showing the design is most likely to be very effective. The temperature rise through the copper rod was approximately 6°C, and the temperature of the steel tube would vary from -192°C at the copper rod to 10°C at the flange. While it is important to note that the simulation is an idealized scenario, the results suggest that the design will perform very well as the temperature results of the simulation will likely not deviate far from the truth.

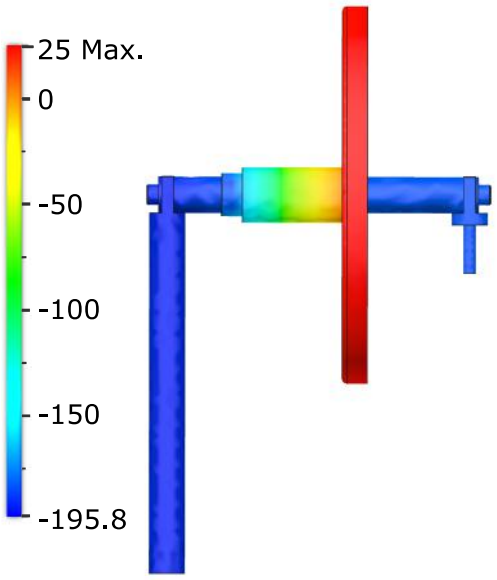

Figure 3.18: *A heatmap of the thermal simulation result.*

3.2.4 Temperature regulation

To perform consistent cryo-EBID experiments with this setup, a reliable system for regulating the stage temperature is needed. This could be established by implementing a PID temperature controller, a device widely used in all sorts of temperature regulation systems. A PID temperature controller continuously monitors a temperature and adjusts an output to accurately control a system's temperature using a Proportional, Integral and Derivative (PID) control algorithm. For our purpose, the PID controller would read the temperature from the PT-1000 while the output is wired to the heater with cooling power provided through the cold finger.

Due to its size, the PT-1000 was hard to mount on the stage without damaging the leads or creating a short. This was resolved by crimping the

leads into two female pin connectors and encapsulating the whole component in Teflon shrink tubing, this was then secured to the stage using a generous amount of silver epoxy. The wires connecting to the PT-1000 and heater were equipped with corresponding male and female pin connectors, allowing the wires to be easily detachable.

Figure 3.19: *(a): CryoCon 62, (b): Oxford Instruments ITC 503, (c): Jumo Quantrol LC100*

Three temperature controllers were considered. First, the CryoCon 62 cryogenic temperature controller, which was lying unused in storage. Specifically designed for cryogenic applications, it featured a low sensor power dissipation of only a few micro-watts. the sensor power dissipation is the heat generated by measuring out a temperature sensor. Unfortunately, it turned out there was an irreparable issue regarding the microcontroller which permanently disabled the feedback output, rendering the CryoCon unusable for use as a temperature controller.

The second option was the Oxford Instruments ITC 503 Intelligent temperature controller, likewise found among the old stored equipment. The ITC 503 was also a lab-grade temperature controller capable of measuring temperatures with very little power dissipation. Since the ITC 503 came out in 1993, it was older than the USB interface and thus incompatible with any modern computer. The ITC featured an obsolete 25-pin RS232 serial port, which we could connect to USB using a triplet of different converter cables. After contacting Oxford for the only software package available for configuring an ITC 503, it became apparent that the software was not compatible with 64-bit graphical drivers, rendering a connection to the ITC impossible.

Since there were no more viable options available, we acquired a brand new Jumo Quantrol LC100 temperature controller. The LC100 is a compact

PID temperature controller designed for general temperature control applications, featuring a power dissipation of approximately 10 micro-watts and a temperature range down to -200°C which was well suited for our specific setup. The output consisted of a relay, an electrical switch which is connected in series with the heater which is powered by a separate 60W AC to DC power supply. Although the resistor is rated for 50 Watts of continuous power, as after that the resistor body will not transport the heat quickly enough to prevent overheating, a 60 watts power supply would not pose a problem as the temperature controller would prevent the resistor from reaching over the maximum rated temperature of 155°C. The LC100 also features a built-in auto-tuning method for tuning the PID parameters, the controller tunes the parameters using the Ziegler-Nichols algorithm [10].

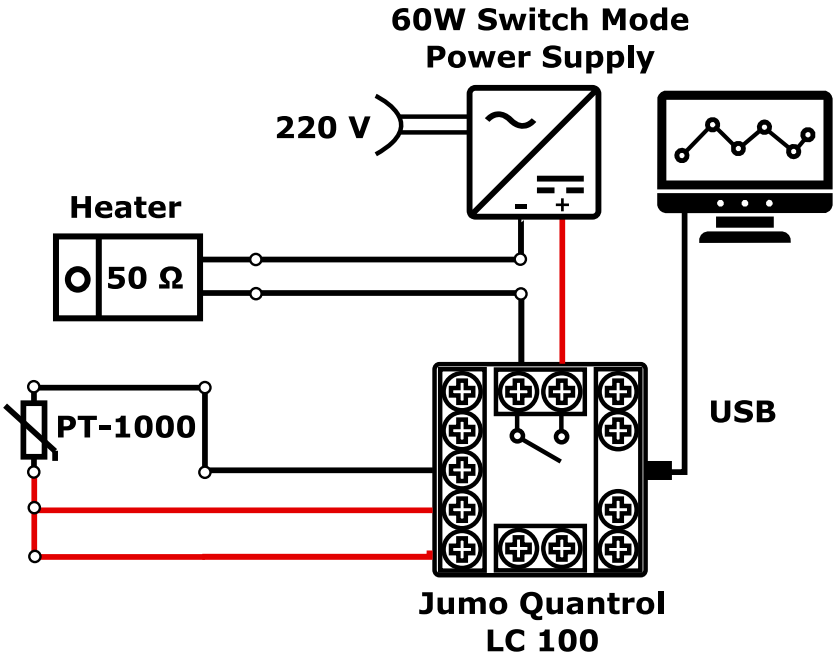

Figure 3.20: *The electrical diagram for the temperature regulation setup*

The Temperature controller connects to the computer via USB and makes use of the RS485 Modbus RTU protocol, a communication protocol mainly used in industrial control systems. the Modbus RTU protocol is a 'request-response' or 'Master-Slave' protocol, where the computer (master) sends a request to connected devices (slaves), and the slaves send a response accordingly, such as when the master requests stored data of the slave device. The communication from a computer to the temperature controller is done using the Minimalmodbus module for Python [3], which allows

Python code to initiate requests to connected devices via a USB serial connection.

I created a Python class using minimalmodbus for initiating the necessary requests and integrated this class in Python code which includes a custom-made Graphical User Interface (GUI) built using the TKinter Python Module. The GUI allows for live plotting of the temperature, set point and output data, real-time adjusting of the temperature setpoint and saving the temperature data in a .csv format with an according screen capture of the GUI for reference.

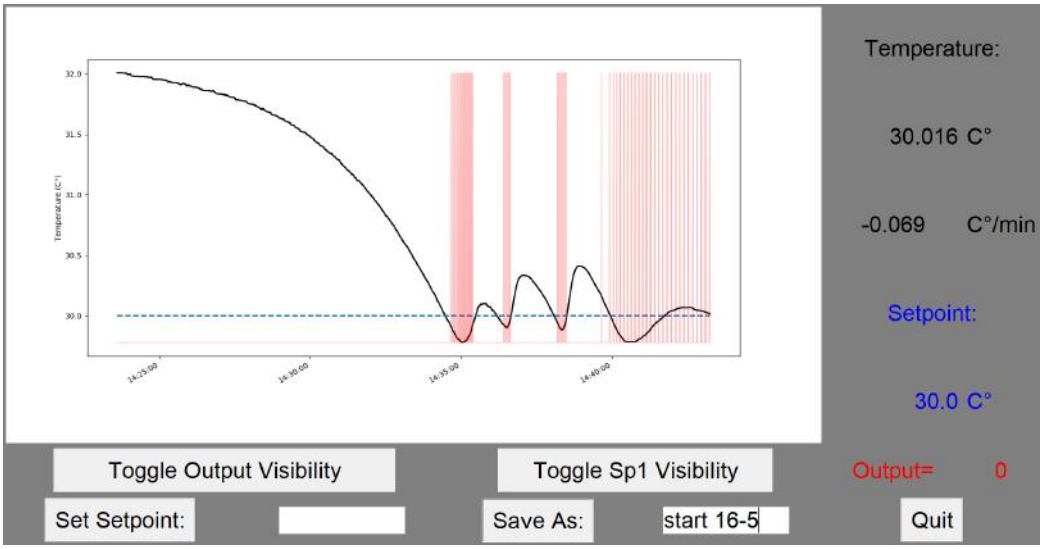

Figure 3.21: *The temperature controller GUI featuring live plots of the readout temperature (black line), the temperature setpoint (dotted blue line) and the controller output (Red). The controller is seen stabilizing the temperature to 30°C.*

3.3 Testing and calibration

3.3.1 Ex-situ testing

Before making any modifications to the SEM, it was crucial to assess the thermal performance of the stage. Therefore, the stage was tested outside of the SEM. This meant the stage would not be in a vacuum and would thus absorb thermal energy from the air and insulation material, potentially impairing the thermal performance of the stage. Conducting tests in a so-called 'ex-situ' environment provided a baseline for the stage's thermal performance, indicating its behavior in a vacuum chamber. To simu-

Version of June 28, 2023– Created June 28, 2023 - 15:33

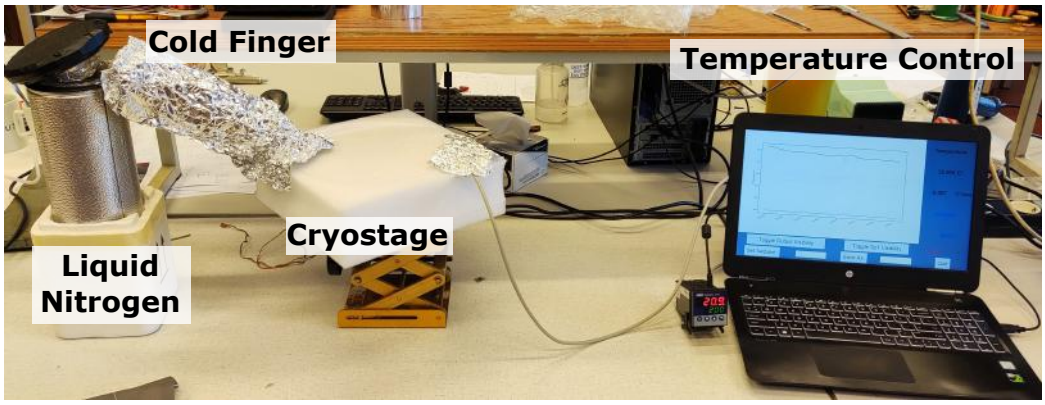

Figure 3.22: *The in-air test setup*

late a vacuum environment as closely as possible, the stage was insulated thoroughly by placing it in a foam box encased with bubble wrap plastic. The cold finger was also encapsulated in multiple layers of bubble wrap and aluminum foil. Additionally, the setup was made airtight to prevent convective air movements, which minimized the formation of condensation ice. The lug on the other end of the cold finger was submerged in liquid nitrogen, simulating a cooled thermal feedthrough.

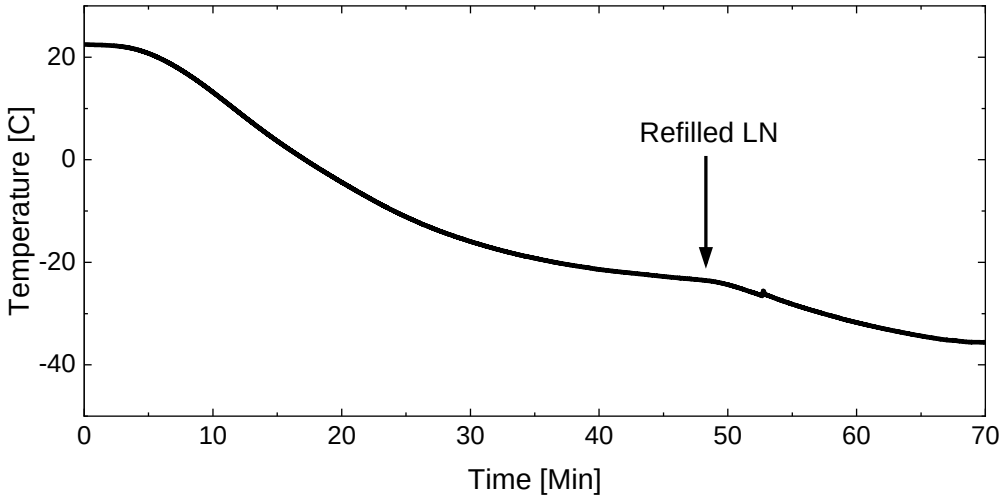

Figure 3.23: *The ex-situ temperature development.*

The temperature logging of the stage started immediately after placing the other end of the cold finger in the liquid nitrogen. The stage started cooling down quickly, having reached the maximum cooling rate of approximately -1,5°C/min after ten minutes of cooling, it showed a typical

exponential decay, as expected of a cooling body. After fifty minutes, the temperature appeared to stabilize at approximately -22°C. I observed that the liquid nitrogen level had fallen too low for the cold finger to be in contact with it so it was refilled which made the temperature lower further to -35°C. The eventual goal was for the stage to reach -50°C, but with a noticeable cold draft emanating from the setup and considerable forming of condensation ice on the cold finger, it was evident the setup was losing cooling power to its surroundings. These results suggested that the cryostage would be able to reach -50°C in a vacuum.

3.3.2 In-situ testing

Component cleaning Before use in the vacuum chamber, all components were thoroughly cleaned and all surface contaminants were removed.

1. **Cleaning of components (except flange):**
    - The components were cleaned with a 15-minute ultrasonic acetone bath heated to 50°C.
    - This was followed by another 15-minute ultrasonic bath heated to 50°C, using Isopropanol
    - The components were dried using an N_2 gun.
2. **Cleaning of the cold finger:**
    - The cold finger was first subjected to the same procedure as all other components.
    - Due to the high surface area of the cold finger braid, it was air-baked at 175°C overnight for 15 hours. This procedure created an oxide layer covering the entire copper braid.
    - To remove the oxide layer, acetic acid was applied to the contact points on both ends of the cold finger to improve thermal conductivity.
3. **Cleaning of the flange:**
    - The flange underwent a 30-minute cleaning process in an ultrasonic bath filled with an alkaline washing solution.

Thermal feedthrough flange After cleaning the setup, and installing the feedthrough in the chamber wall, the vacuum chamber was pumped down normally and tested for possible air leaks. Afterward, the electron beam was activated using the maximum electron energy of 30 keV and electron current of 0.41μA. A Thermo Scientific™Mini 900 Scintillation Monitor was used to test for potential X-ray leakage through the flange, but the detector showed no significant change compared to the background noise, confirming that the flange was impermeable for the emitted X-rays of the SEM.

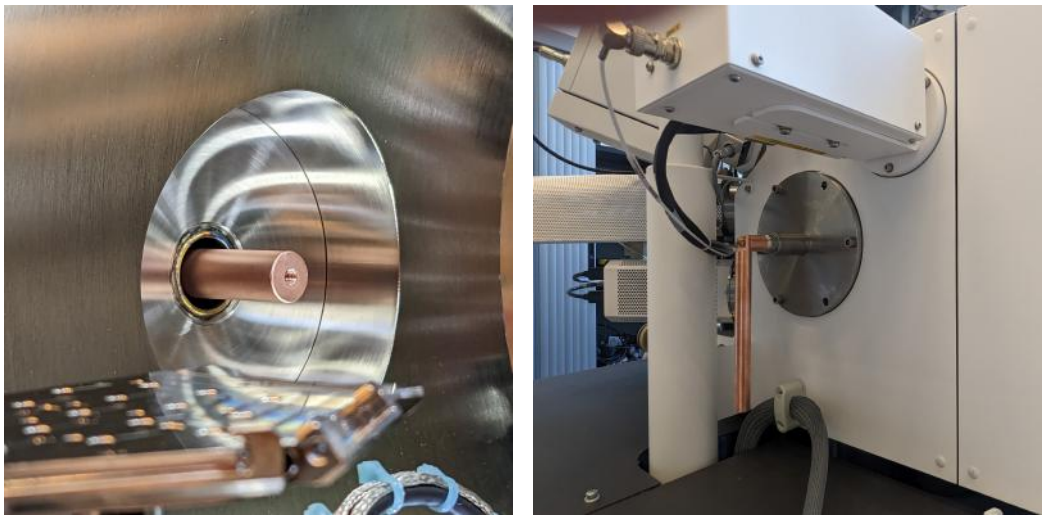

Figure 3.24: *The thermal feedthrough installed in the sem wall. (Left): View from inside the SEM chamber. (Right): View from outside the SEM chamber.*

Imaging thermal leakage Before pumping down, we checked the thermal contact between the cryostage and the sample stage. This was done by using the heater to bake the stage at 70°C and taking images using a handheld FLIR infrared thermal camera to visualize the thermal flow of the setup. A clear temperature gradient was observed along the PEEK feet, showcasing their isolating properties and ability to limit the thermal transfer to the sample stage. In contrast, the thermal transfer to the cold finger appeared to be significant. The thermal imaging indicated the cryostage would perform well under vacuum conditions.

Figure 3.25: *Thermal imaging of the stage being heated to 70°C using the heater from a side-view. A temperature gradient is seen in the feet, indicating a high thermal resistance. Most heat is seen to be conducted away through the cold finger.*

Cryostage performance

Vacuum pressure It should be noted that during optimal conditions or without a sample in the chamber, the chamber should pump down to a pressure of approximately 2.0 E-6 mbar.

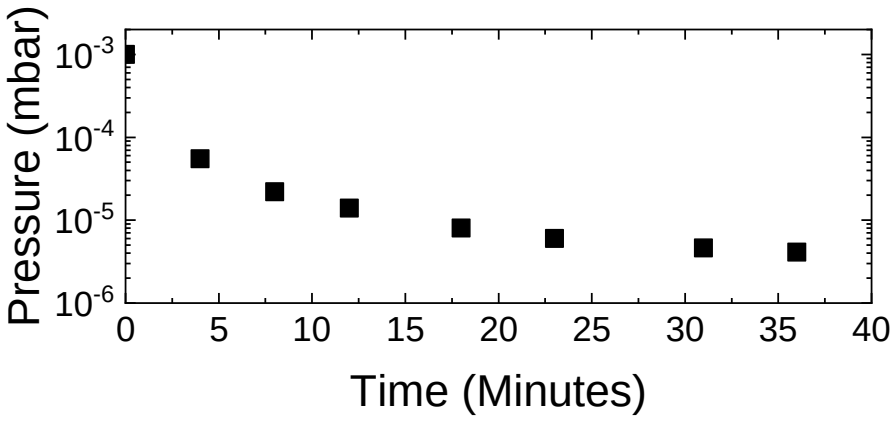

Figure 3.26: *Pressure-time plot of the vacuum chamber loaded with the cryostage*

With the whole setup fitted in the vacuum chamber, the chamber was able to pump down to 4.10E-6 mbar in thirty minutes, roughly double the pressure the chamber reaches without the stage. This is likely due to the outgassing of airborne contaminants which adhere to the stage and cold

finger.

This pressure was not optimal but falls within an acceptable range, it was expected to decrease to a more favorable level after cooling down. This drop is caused by a process known as cryopumping, where a material with an extremely low temperate is introduced in the vacuum chamber to condense and trap contaminant gasses on its surface, resulting in a cleaner vacuum environment.

In our system, the copper rod of the thermal serves as the cryopump. Since the feedthrough is cooled earlier than the cryostage, it is expected to capture a significant portion of the contaminant gasses. Therefore, the impact of cryopumping on the stage itself is likely minimal. This was confirmed, as soon as the feedthrough was cooled down, the system was able to achieve a vacuum pressure of 1.25E-6 mbar.

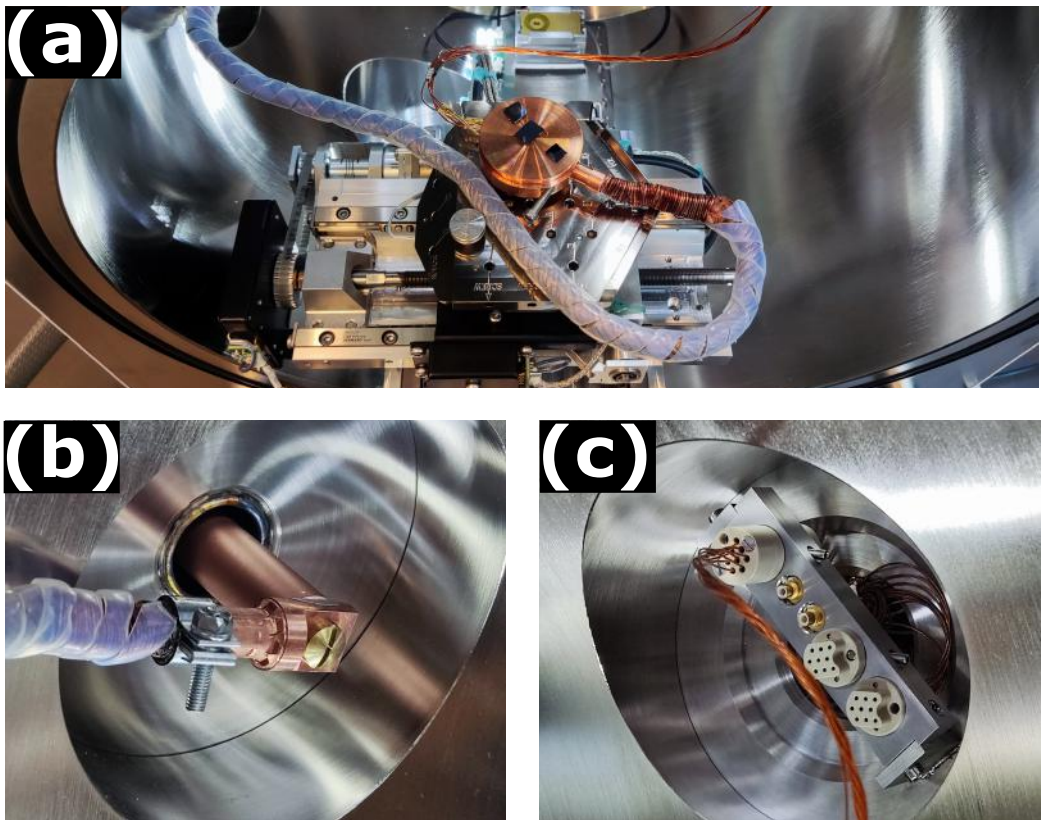

Figure 3.27: *(a): The cryostage loaded placed on the sample. (b): The cold finger connected to the thermal feedthrough. (c): The electrical cable connected to the electrical feedthrough.*

Cooling performance The following procedure is undertaken when cooling down a sample

1. Prepare a sample on a copper sample stub and place it on the cryostage.
2. Connect the cold finger and electrical wires to the cryostage.
3. Vent the vacuum chamber.
4. Move the sample stage to the following coordinates: (x,y,z,R[†]) = (0,0,0,0)
5. Place the stage on the SEM sample stage as seen on3.27(a), Pushing the pins all the way down.
6. Screw the cold finger on the feedthrough horizontally pointing towards the chamber door with a thin indium foil between the contact interface, as seen in Figure 3.27 (b).
7. Connect the 9-Pin C-sub connector to the electrical feedthrough as seen in Figure 3.27 (c).
8. Close the vacuum chamber and start pumping the chamber.
9. While the chamber is pumping down, set up the temperature controller and Python GUI software.
10. Connect the thermal anchor to the feedthrough, positioned inside the cryogenic dewar flask and apply a generous amount of Apiezon™N grease on the contact interface for a better thermal transfer.
11. Place polyester wool under the whole setup to catch spilled nitrogen and condensation water as seen in 3.28.
12. Wait for the chamber pressure to reach under 5E-5 mbar.
13. Start a measurement with the temperature controller GUI software.
14. Set the temperature controller to a desired temperature.
15. Fill half the dewar flask with liquid nitrogen
16. Once the thermal anchor has cooled down past the point of the Leidenfrost effect [El-Dardiry], carefully fill it almost to the top and refill when needed.

[†]R refers to the rotation of the stage and is expressed in degrees

17. Wait for the temperature to reach the setpoint.

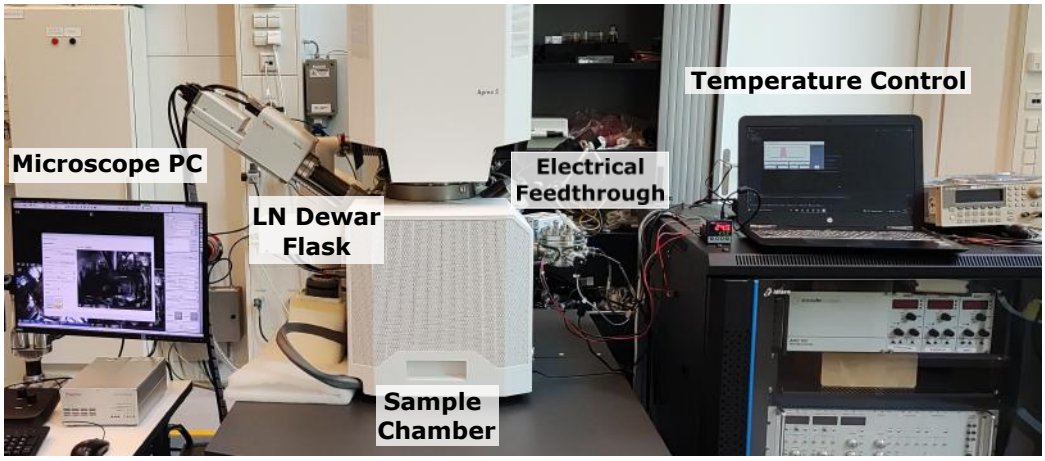

Figure 3.28: *The full setup outside the SEM chamber when performing cryo-EBID experiments.*

When adding liquid nitrogen to the dewar flask, it takes approximately four minutes for the thermal anchor to cool down past the point of the leidenfrost effect and ten minutes to observe a decrease in temperature in the cryostage. As expected, the cooling performance is improved when the setup is in a vacuum environment and the maximum cooling rate improved from -1.5°C/min to -2°C/min. The time for the stage to cool down is in an acceptable range, the stage can cool down from room temperature to -50°C, which is the temperature cryo-EBID is performed at, in approximately 60 minutes, see Figure 3.29. After depositing, the stage can be heated up and an impressive rate, being able to heat back up from -50°C to 30°C in 8 minutes and reach a maximum heating rate of approximately 13°C/min.

However, some artifacts remain without explanation. The sampling time should remain constant at 200ms. Instead, there is a noticeable uptrend caused due to an increased processing time for a constantly growing data set when performing a measurement. The sample time also displays a seemingly periodic jumps of unknown origin. These artifacts do not jeopardize the actual temperature values so creating deposits was prioritized over optimizing the code due to the limited time frame of the project.

Thermal drift Due to the temperature change, the SEM image could be subjected to thermal drift. Thermal drift is the phenomenon where the sample drifts due to thermal expansion or contraction within various in

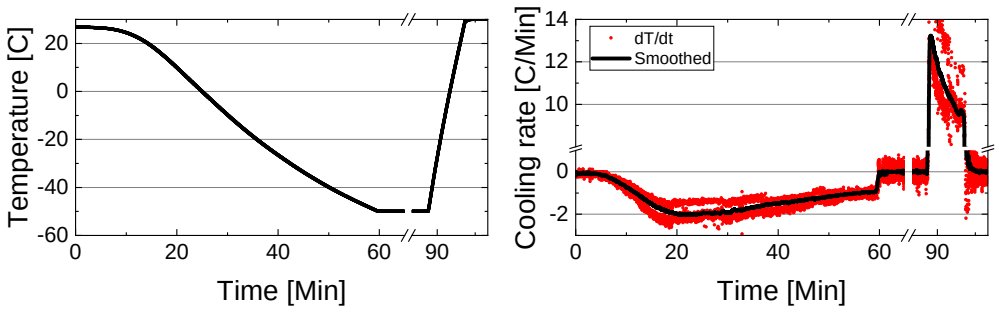

Figure 3.29: *A typical temperature development for a cryo-EBID session, cooling down and maintaining a temperature of -50°C and heating up afterwards.*

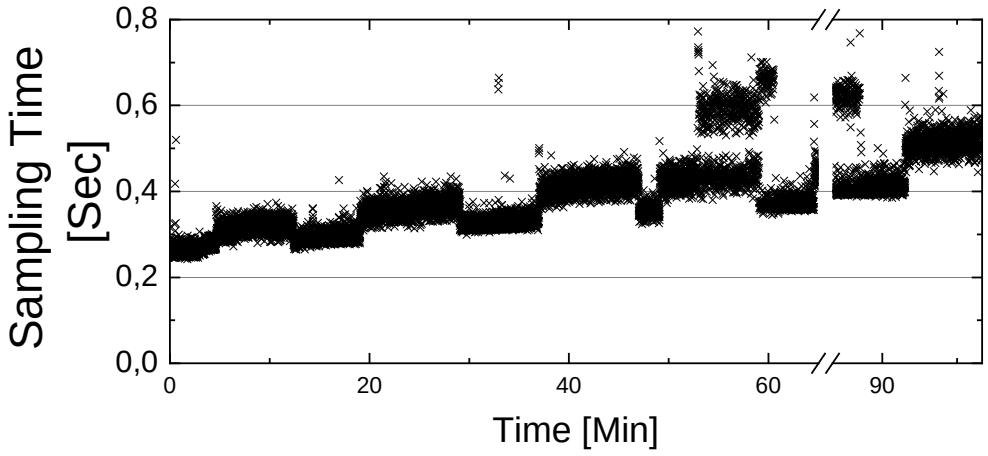

Figure 3.30: *The sampling times for Figure 3.29.*

parts of the SEM, resulting in a temperature-dependent displacement of the SEM image. This displacement is dependent on multiple factors such as sample location and change in temperature. This was tested on a dust particle placed approximately half a radius away from the center on the large 38mm stub and with a change in temperature of 30°C, a drift of approximately 11μm was observed. This test only served a qualitative purpose, assessing the approximate magnitude of the drift and if it was indeed significant. The results indicated that during a thermal cycle, the sample could displace on the order of micrometers. This drift will likely not interfere with cryo-EBID experiments but should be taken into account.

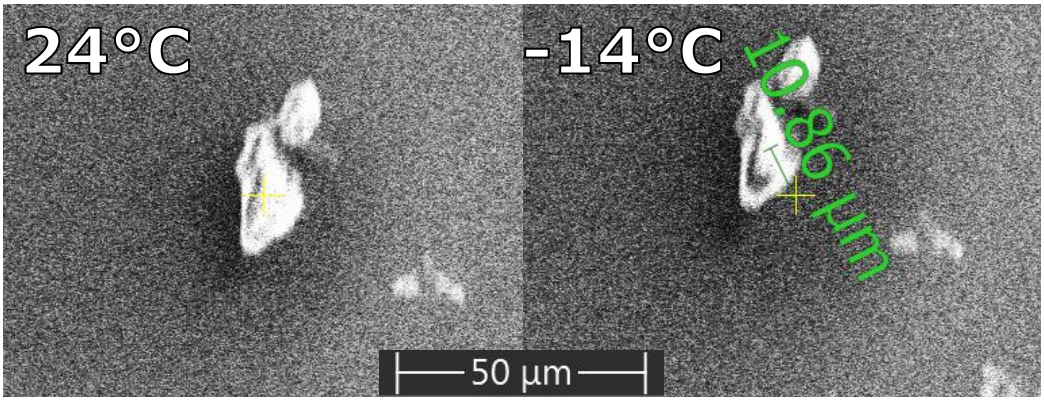

Figure 3.31: *Observed thermal drift on a dust particle for a ΔT of 30°C*

Chapter 4

Performing Cryo-EBID

4.0.1 Experimental procedure

Cryo-EBID was carried out using the following procedure:

1. Cool down the stage using the standard cooling procedure.
2. Focus the electron beam at a 20.000x magnification.
3. Z-link the system and set the distance between the sample and Pole Piece at 10mm.
4. Locate desired deposition area and refocus the beam.
5. Create or Load a pattern for the SEM to pattern on the substrate.
6. Turn on the beam deflector to avoid exposure to the substrate.
7. Heat up the precursor in the GIS, the precursor is heated to 50°C.
8. Insert the GIS needle.
9. Open the GIS for 30 seconds.
10. Retract the GIS.
11. Write the pattern.
12. Heat up the cryostage to 30°+ C.
13. Turn off the beam deflector.

Except for the dwell time and beam current, all deposits were made using the same parameters: GIS opening time: 30s, Electron energy: 15 keV, sample distance: 10mm, beam pitch: 10mm, temperature = -50°C, chamber pressure (with cooled setup): approx. 1.5 E-6 mbar, Passes: 1. All depositions were made on Silicon Oxide substrates, which underwent two 15-minute ultrasonic baths, first in acetone and then in isopropanol.

The sample distance must be 10mm, the GIS is calibrated such that this distance between the sample and the GIS needle is 100 μm. A pattern can consist of various shapes and elements with different electron beam parameters, except for the electron beam current. If parts of a pattern require different electron beam currents, a part of the pattern must be selected and patterned with the desired electron beam current, manually select another part of the pattern and change the beam current and pattern it. This is unfortunately a limitation in the microscope software and could not be resolved.

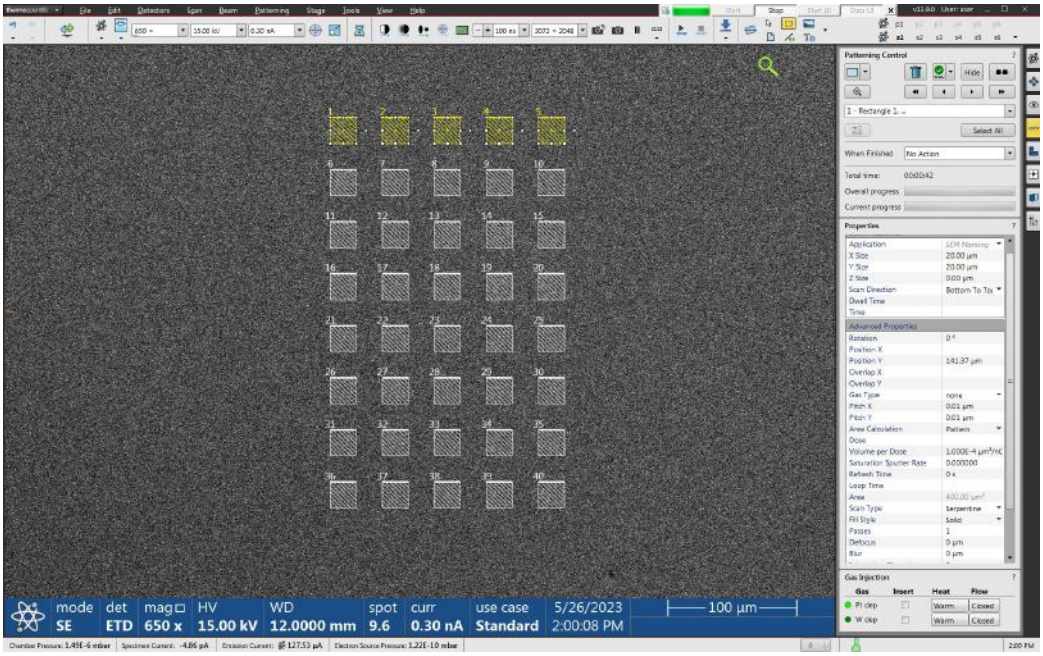

Figure 4.1: *A 5x8 square pattern being created in the microscope software.*

4.1 Squares

To find the optimal parameters for writing nanowires, we printed a grid of squares with varying beam currents and dwell times. The last row of an 80 nA beam current was not patterned right due to the GIS needle obstructing the area, this was caused by incorrect calibration of the GIS needle.

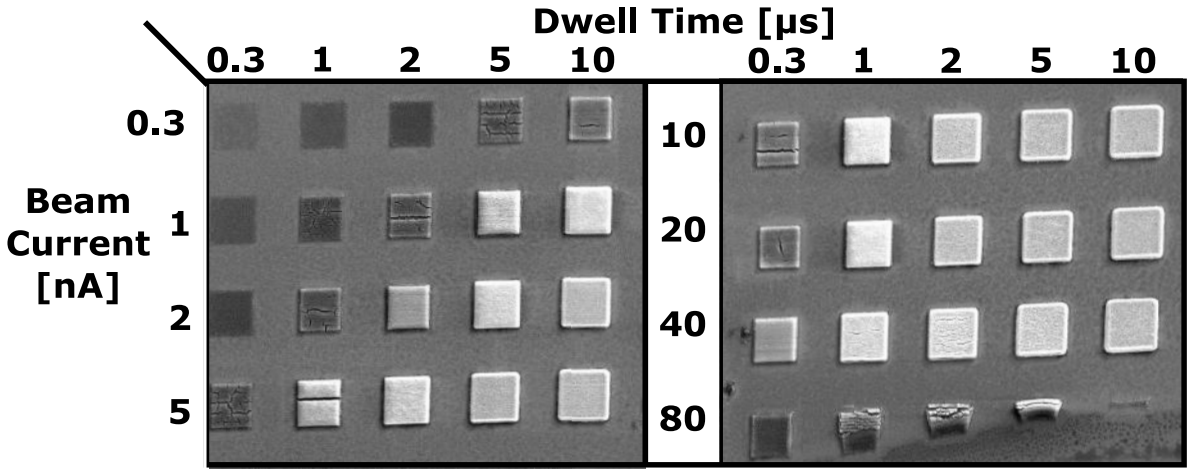

Figure 4.2: *the 5x8 grid pattern of 20x20 µm squares featuring varying dwell times and beam currents. From left to right, the patterns feature the following patterning times: [800ms, 3s, 6s, 14s, 28s].*

Morphology

The squares can be categorized to fall into three regimes, with the first regime being the insufficient-dose regime. In this regime, the area was not irradiated sufficiently, resulting in porous deposits which are very prone to cracking, indicating that only a layer on the bottom of the condensate was dissociated. These cracks are possible due to non-disassociated precursor quickly leaving the deposit 4.4. The second regime is the sufficient-dose regime, where the area received enough dose to dissociate precursor in most of the condensate layer, displaying a smooth surface. The third regime is the excessive-dose regime, where the high electron dose causes beam-induced heating in the deposit. This heating causes shrinkage due to the evaporation of undissociated precursor, cracking the deposit.

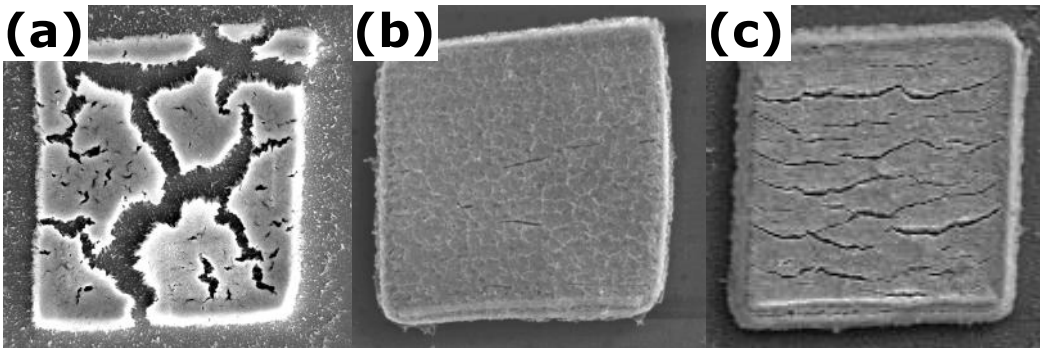

Figure 4.3: *20x20 µm squares at varying electron doses. (a): insufficient-dose regime. I_{beam} = 710 pA, dwell time: 2 µs. (b): Sufficient-dose regime. I_{beam} = 20 nA, dwell time: 10 µs. (c): Excessive-dose regime. I_{beam} = 40 nA, dwell time: 10 µs.*

Surface adhesion

We did encounter the problem of poor surface adhesion, the deposits would peel off or vanish from the substrate. This problem is likely due to incomplete dissociation near the surface of the substrate and the aforementioned beam-induced heating, which causes the deposit to shrink and peel off the substrate. The surface adhesion appeared to improve with an increasing dose, benefiting more from an increase in dwell time than beam current as an excessive current caused the deposit to crack. The increase in dwell time lead to a higher degree of dissociation with less beam-induced heating, leading to a more rigid deposit which was more resistant to shrinking.

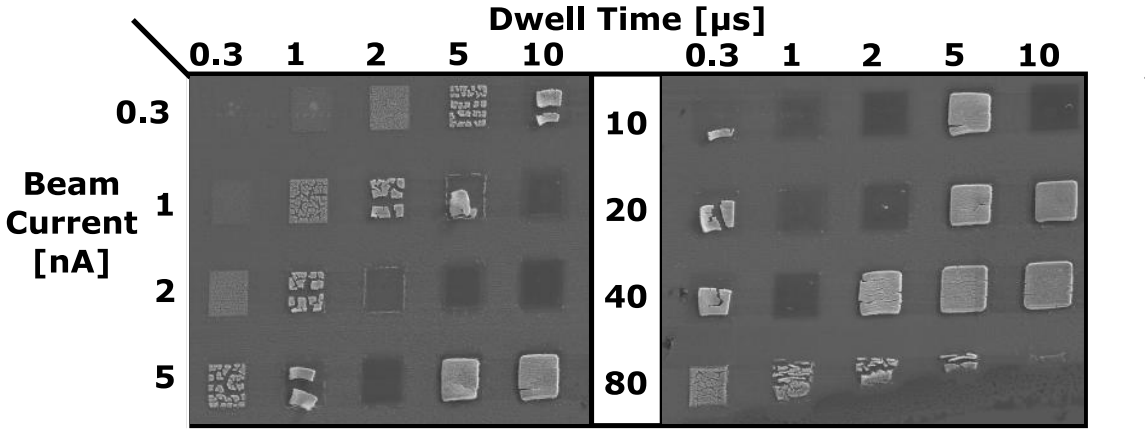

Figure 4.4: *The square grid after being exposed to the electron beam while live-imaging, all squares display some form of shrinking or breaking.*

A different, but unexplored, possible method of improving the structural rigidity of the deposits is to decrease the reheating rate of the stage and reheat to a higher temperature (e.g. 100°C). This might allow the undissociated precursor to leave the deposit more slowly, and slow down the shrinking process when reheating the deposits. Baking the deposits could evaporate undissociated precursor slowly en evenly, reducing the shrinkage caused by beam-induced heating. Unfortunately, we were not able to explore these options within the time frame of this project.

4.2 Wires

Grid scanned depositions The deposition parameters which appeared most promising for the nanowires were an I_{beam} of 20 nA and a dwell time of 10 μs of which the deposit can be seen at 4.3(b). This deposit displayed the least surface roughness and withheld its shape most after irradiation.

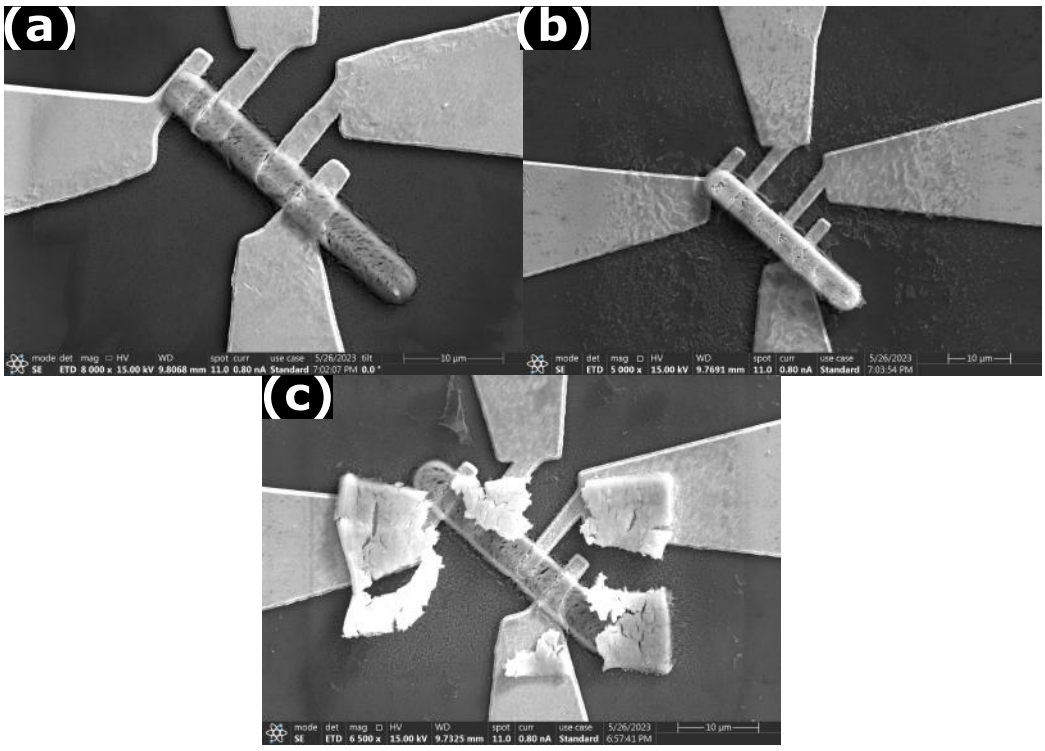

Figure 4.5: *5x30 micron deposits.*

The nanowires were to be deposited onto four thin-layer gold probes connected to gold contact pads, a thin wire could be wirebonded to these

contact pads to allow for a four-point resistance measurement to be performed on the nanowires. The wires were rectangular deposits 5 microns in width and 30 microns in length. Out of the five wires intended to be deposited, only three were deposited successfully. The Cryo-EBID process does not allow for real-time imaging after opening the GIS. Therefore, one needs to wait until after the reheating to observe their deposits.

Since the areas for the nanowires are separated by hundreds of microns, these locations are saved in the SEM in the form of coordinates. the stage must be repositioned to the next saved location between each deposition. This repositioning is subject to thermal drift and stage movement hysteresis, resulting in minor inaccuracies when moving to a saved location. Repeatedly moving between saved locations could eventually move the entire deposit by microns. which could cause a deposit to be in the wrong spot. This shift is responsible for the differences in placement observed in Figure 4.5, it is uncertain whether this shift is the cause for the misplaced deposit shown in Figure 4.6(b) or if the deposit had detached itself from the substrate. The top of the structure resembles the porous interior structure of a deposit, suggesting the deposit has become detached and flipped over.

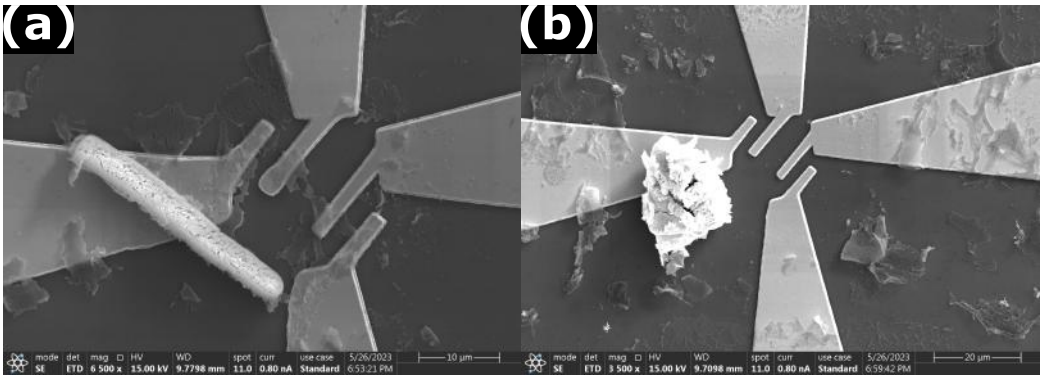

Figure 4.6: *The unsuccessfully patterned nanowires*

An error in the GIS had caused it to falsely indicate the precursor was heated, therefore it was unknown whether the precursor was released and a deposition had been made. This misconception led to two accidental exposures of the precursor due to live imaging. In Figure 4.5(c), a deposit was observed on top of a patterned nanowire which quickly disintegrated after heating induced by the beam. In Figure 4.6(b), whether a nanowire was present on the contacts is unknown.

Line-scanned depositions The first set of wires were patterned using grid scans, where the deposit was made on an area on which the electron beam scanned the area in lines from top to bottom. It would be more beneficial to create wires using line scans as this would simplify the patterns greatly. However, the overlap between each element is about twice as small as in a grid scan which would change the parameters needed for a good deposit.

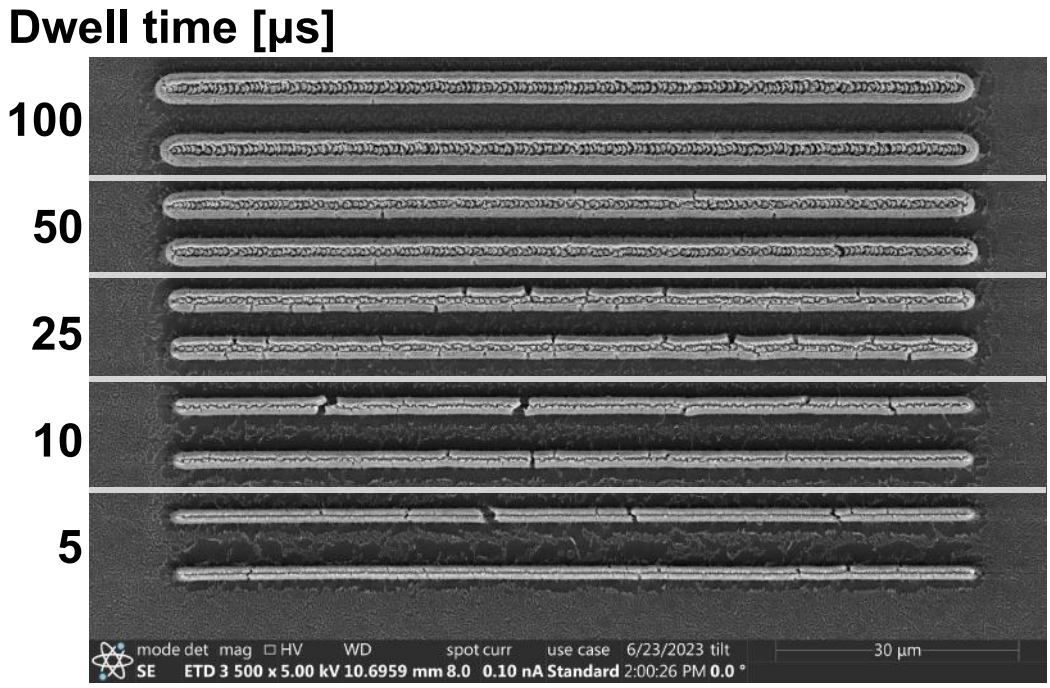

Figure 4.7: *Beam pitch = 5nm, GIS opening time = 30s. From top to bottom, the total deposition times are: 2s, 1s, 0.5s, 0.25s, 0.125s.*

To compensate for the decrease in overlap, a higher dwell time was proposed. To test whether an increase in dwell time would result in better results, ten wires were deposited with the same parameters as in 4.5 but at five different dwell times. The original dwell time of 10 μs indeed seemed to result in an insufficient dose when depositing using a line scan. A higher dwell time did prove to be necessary to accommodate for the lower overlap, a dwell time of 100μs appeared to be most suitable as it resulted in the only deposit which held its shape without any breakage.

It appears the line scan did result in a too-large electron dose as the wires appear to break in the center line where the electron beam hits the precursor. We hypothesize the beam results in heating of the deposit,

breaking them in the center while the edge remains intact. The edge of the deposit received a lower dose as they are formed by backscattered electrons which leave the substrate at an angle.

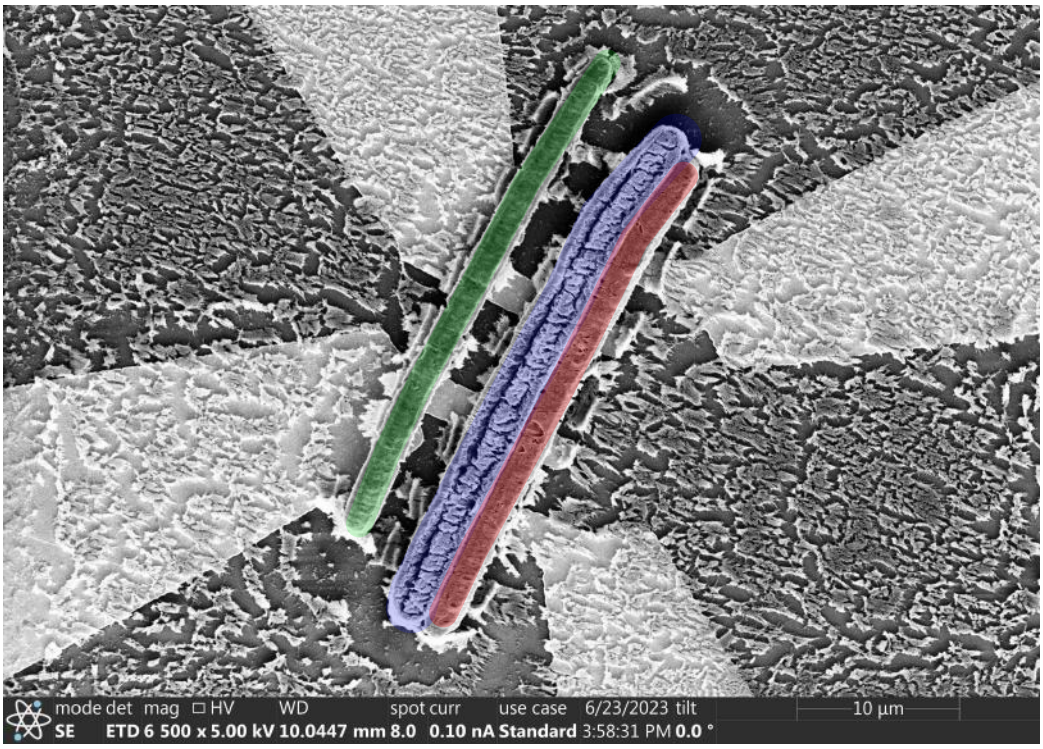

Figure 4.8: *Three wires printed on the same gold probes with different beam currents. (Blue): 14 nA. (Red): 12 nA. (Green): 8 nA. GIS opening time = 45s*

A beam current of 20 nA was deemed too high for depositions using a line scan. Therefore, eight different beam currents were used ranging from 20 to 6 nA. The GIS was opened once during the whole deposit as we expected the precursor to spread out over the substrate. But unfortunately, the precursor did not spread enough, resulting in a lack of deposits in several spots. There was also an error in the software relating to the positioning of the stage, causing three deposits to be deposited on the same spot, which can be seen in figure 4.8. The deposits used 14, 12 and 8 nA, of which the 8 nA deposit displayed the least damage and the smoothest surface, indicating the 20 nA beam current was indeed too high. These depositions were unfortunately the only ones suitable for performing resistance measurements.

Transport measurements Resistance measurements were performed on nanowires shown in Figure 4.5 and 4.8. Unfortunately, the measured resistance values were on the order of megaohms (MΩ), suggesting the deposits were non-metallic and therefore unusable for use as nanowires. These results can be attributed to the use of incorrect beam parameters, which unfortunately have not been explored enough due to the limited time frame of the project. Only a single session was available for depositing nanowires, limiting the opportunity for optimizing these parameters.

The deposit morphology was also affected by the sub-optimal beam parameters, as opposed to the deposited squares, the nanowires had an inconsistent surface roughness and overall thickness or were not deposited at all. This is likely due to the uneven distribution of the precursor condensate on the substrate considering the relatively large distance between the deposition areas. The GIS was opened for a certain time after which the patterns were deposited relatively quickly, possibly not allowing the condensate to evenly distribute over the substrate. a more controlled and consistent deposition is required to achieve consistent results, possibly involving the additional delivery of precursor to compensate for the uneven distribution and spreading of the precursor during deposition.

Variating pitch and number of passes Variations in the beam pitch and the number of passes were unexplored parameters. The beam pitch represents the distance between each adjacent point in a pattern. The size of each point is determined by the spot size. The 'overlap' refers to the percentage of the area of the electron beam spot which overlaps between each adjacent point. The number of passes refers to the number of times the beam goes over the pattern, this is used in traditional EBID to 'stack' deposits and create freestanding structures. In cryo-EBID, more passes could remove more undissociated precursor molecules from a deposit, strengthening its structure.

We made twelve deposits 50μm in length with three different pitches and four variations on the number of passes. Single-pass deposits and thus very short patterning times, in the order of 25ms, were not possible due to limitations in the software.

No noticeable changes were observed in varying the overlap from 87% to 50%, this can be attributed to the fact that after a minimum of 10 passes, all of the precursor condensate has been dissociated. It appears that after ten passes the maximum deposit thickness has been reached. Unfor-

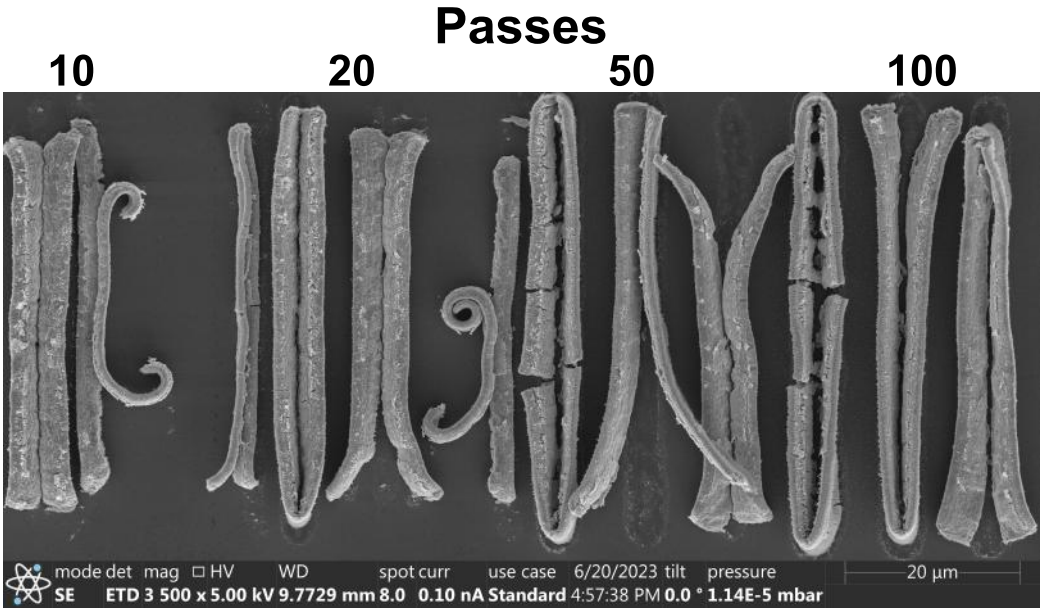

Figure 4.9: *50mum nanowires in triplets with Pitch/Overlap from left to right: 5nm/87% — 10nm/75% — 20nm/49%. Four triplets with the number of passes from left to right: 10 — 20 — 50 — 100. Printing using: I_{beam} = 20nA, E_{beam} = 15keV, T = -50°C, GIS opening time = 60 seconds*

tunately, using multiple passes seems to result in significant damage to the deposits, with most deposits being cut in half, broken in pieces, or detached and curled up, likely due to the successive passes. It appears cryo-EBID depositions need to be made using only one pass and needs a less destructive method for purifying the deposits such as baking or irradiating using a low electron dose.

Condensate growth rate The deposition did allow for measuring the thickness of the deposit. The deposit with an overlap of 87% and 50 passes appears to be cut in half after which one half curled up and fell over, revealing a cross-section of the deposit which is measured to be approximately 1.3 $\pm$ 0,1 *mu* m for a GIS opening time of 60 $\pm$ 5 seconds. This results in a growth condensate growth rate of 21.6 $\pm$ 2 nm/s at a GIS height of 100 microns. We assume that at 50 passes, the full layer of condensate is dissociated as no noticeable increase is seen with an increase of passes.

Chapter 5

Conclusion

In conclusion, we successfully designed and fabricated a functional cryostage setup for performing cryo-EBID experiments which could be integrated into a Thermofischer Apreo 2 SEM. The cryostage was able to cool down to -50°C in 60 minutes and reach its minimum temperature of -80°C within 150 minutes.

Furthermore, we successfully created depositions using the setup, demonstrating its efficacy. However, due to the lengthy design and fabrication phase, limited time was available for optimizing the deposition parameters. The deposits demonstrated sub-optimal conductive and structural properties, rendering them unusable for their intended use as nanowires. Further experiments are required to refine the process parameters which could potentially enable conductive or even superconductive deposits to be produced.

Chapter 6

Acknowledgements

I would like to thank all members of the Lahabi Lab of which everyone has provided me with much support and suggestions during this project. Special thanks to Matthijs Rog who has fulfilled the role of my daily supervisor for continuous support and guidance during the project, Tycho Blom for providing me with helpful advice on EBID, providing me with the necessary samples for performing transport measurements, and performing those measurements on my behalf and Kaveh Lahabi for providing me with the opportunity to work on this project.

I am especially grateful to everyone who has provided me with technical insight and assistance during this project. Luc Wigbout and Marcel Hesselberth have been particularly helpful in this regard by providing me with copious amounts of technical feedback, and suggestions for the design. Luc has also contributed immensely to the integration of the project into the Apreo 2 SEM, making sure everything worked well and safely, which I am very grateful for. I Would also like to thank all members of the Fine mechanical department (FMD) for sharing their technical knowledge and providing valuable insights regarding my designs, I want to give my special thanks to Kenrick de Grijs for personally taking on the fabrication of my parts and Merlijn Camp for completing his work.

I would also like to express my appreciation to the members of the Electronics Department (ELD) for providing me with the necessary equipment and parts and plentiful resourceful suggestions and feedback for everything electrical in my project. I would like to extend my sincere thanks to Peter Numberi for repairing my temperature controller and providing me with a suitable power supply when times were dire as this was the

third temperature controller which had failed on me and taken a week of my time.

Finally, I would like to thank the OpenAI team for providing me with their ChatGPT AI language model, which has served as a tool for detecting overlooked spelling and grammatical errors while writing my thesis.

Appendix

Appendix A

Technical Drawings

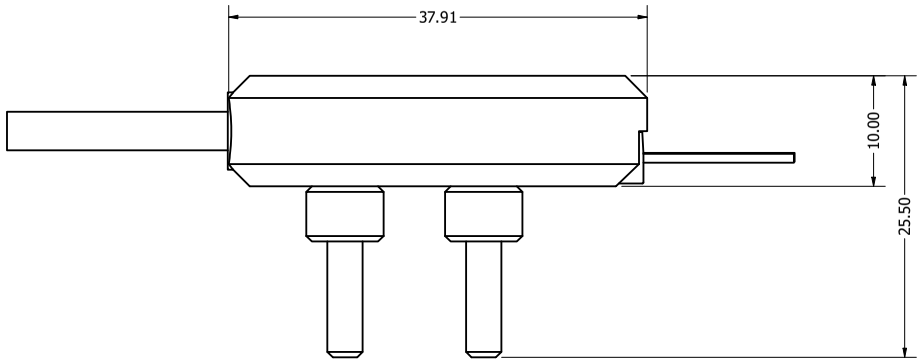

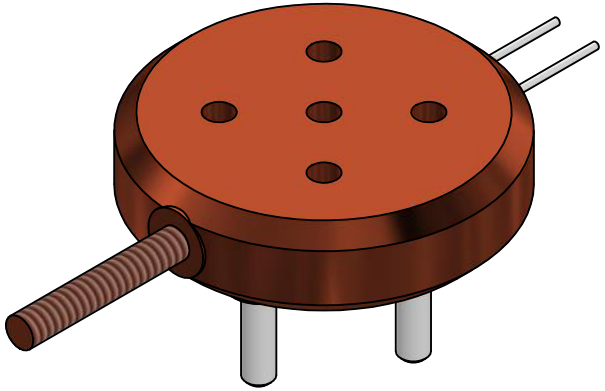

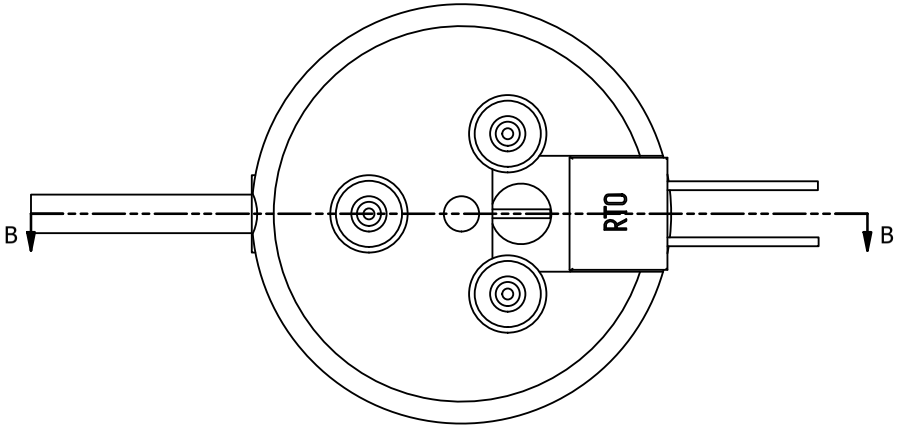

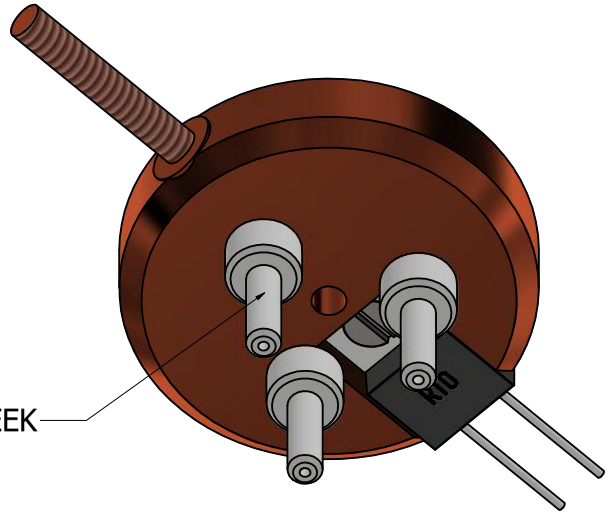

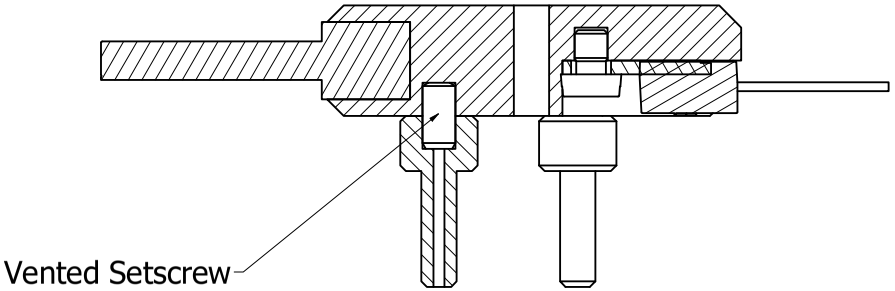

SECTION B-B
SCALE 3 : 1

DRAWN	Bernard Sohl	5-4-2023		
CHECKED			TITLE	Cryo-Stage
QA				
MFG				
APPROVED			SIZE C	DWG NO Final_stage 1 REV
			SCALE 3 : 1	SHEET 1 OF 5

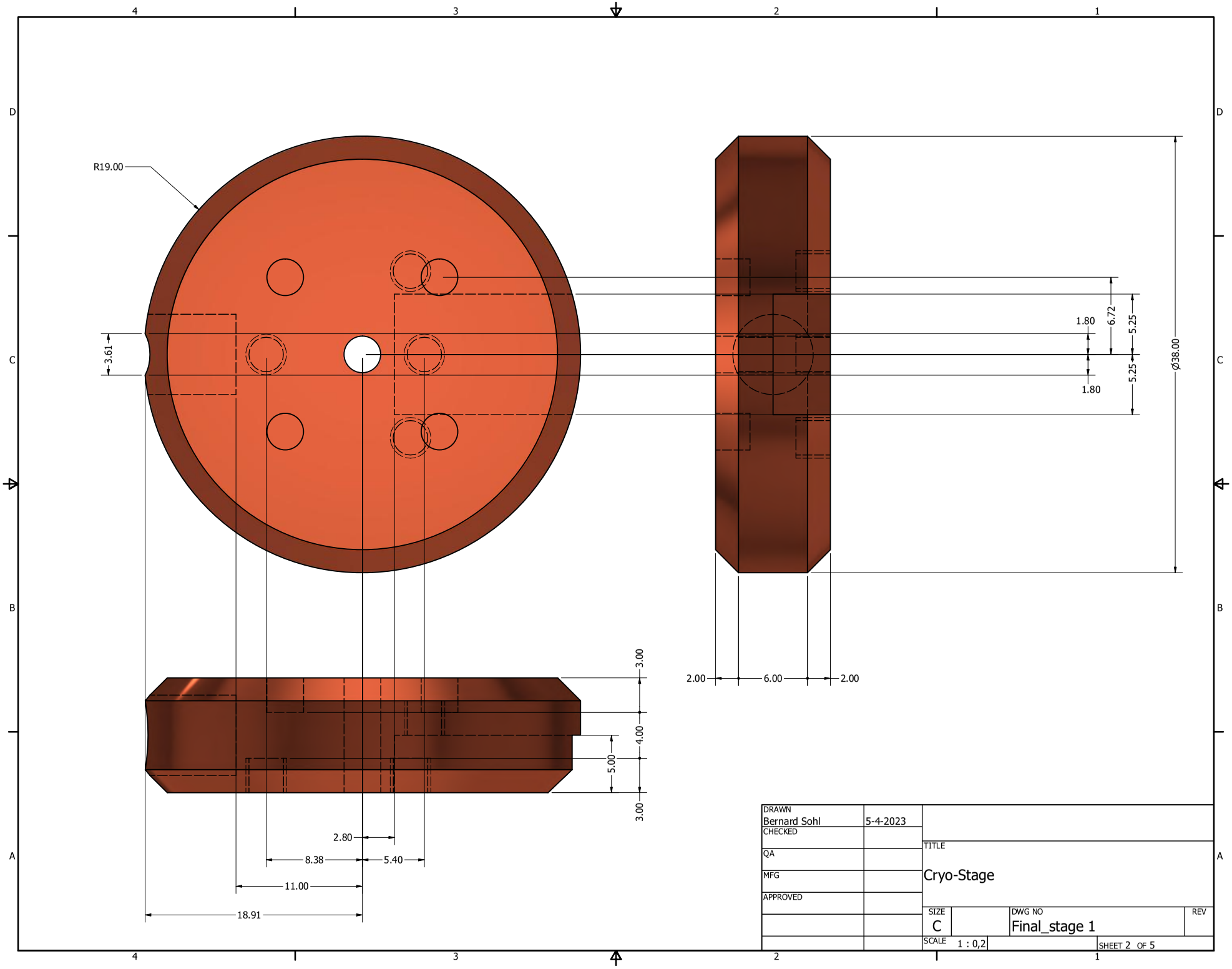

DRAWN	Bernard Sohl	5-4-2023
CHECKED		
QA		
MFG		
APPROVED		

TITLE: Cryo-Stage

SIZE: C | DWG NO: Final_stage 1 | REV:

SCALE: 1 : 0,2 | SHEET 2 OF 5

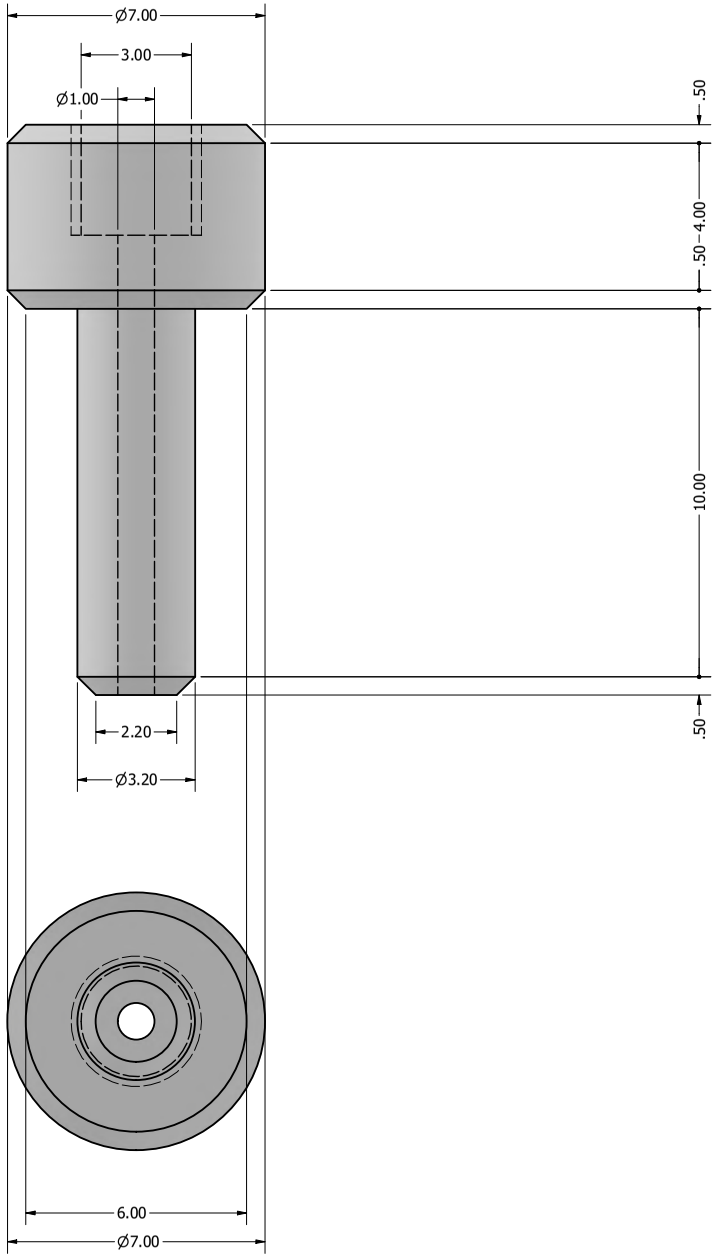

DRAWN Bernard Sohl	5-4-2023	
CHECKED		TITLE: Cryo-Stage
QA		
MFG		
APPROVED		
		SIZE C | DWG NO Final_stage 1 | REV
		SCALE 10 : 1 | SHEET 3 OF 5

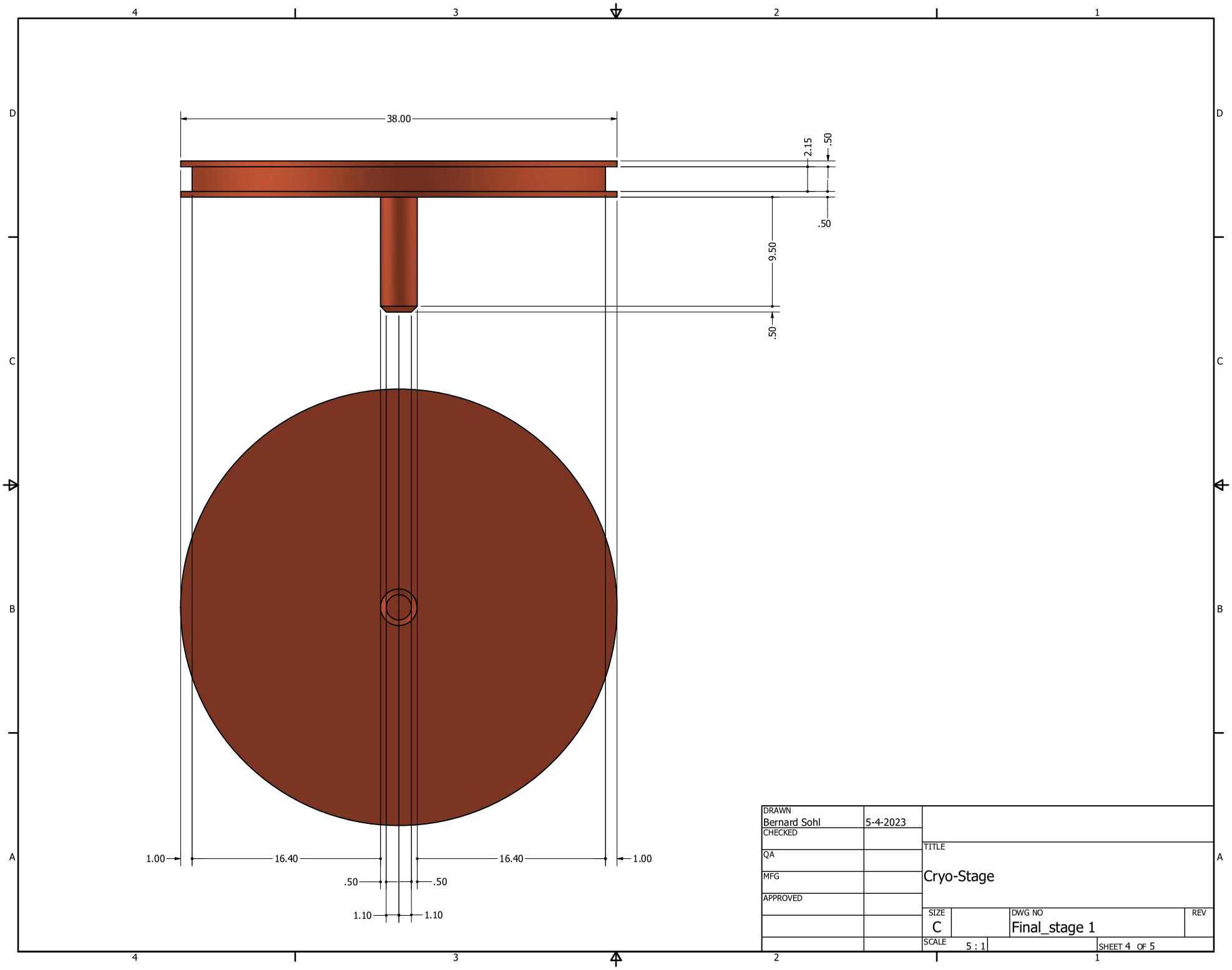

DRAWN Bernard Sohl	5-4-2023	
CHECKED		TITLE: Cryo-Stage
QA		
MFG		
APPROVED		
		SIZE C | DWG NO Final_stage 1 | REV
		SCALE 5 : 1 | SHEET 4 OF 5

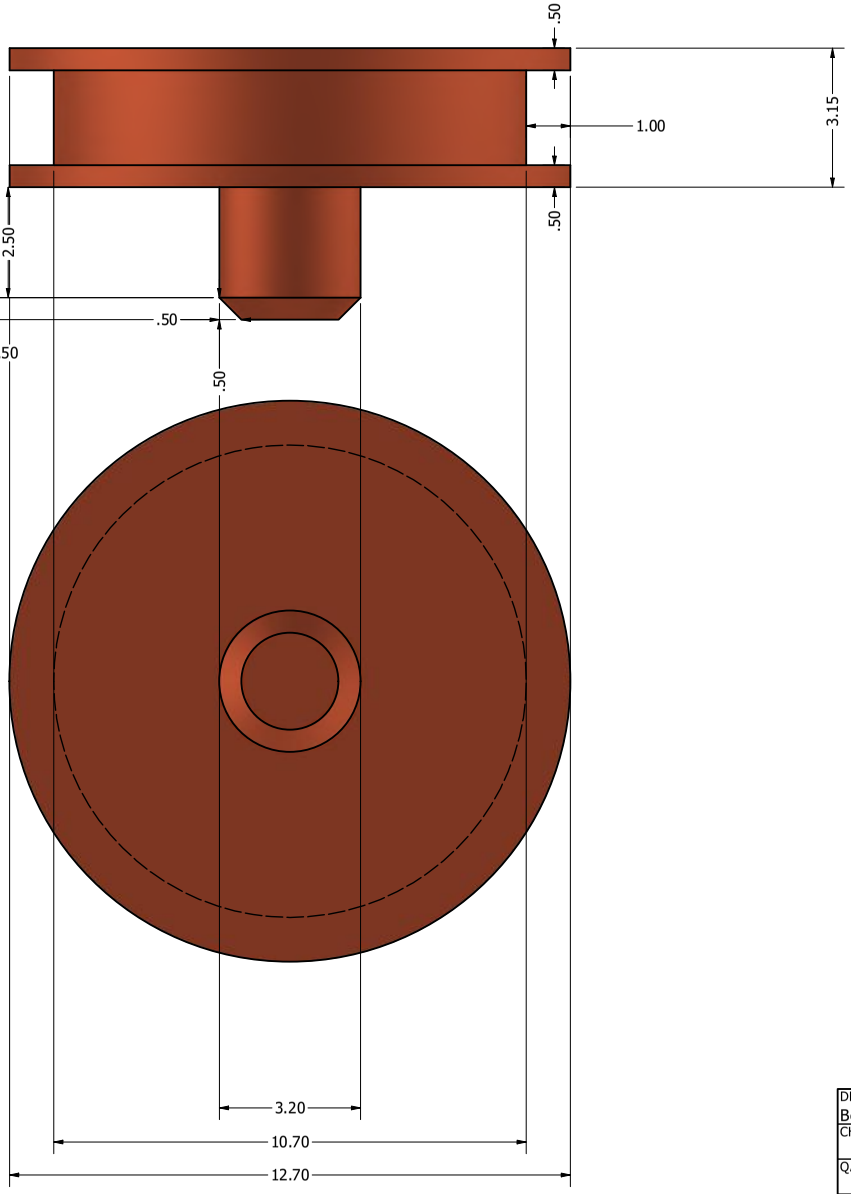

DRAWN Bernard Sohl	5-4-2023	
CHECKED		TITLE: Cryo-Stage
QA		
MFG		
APPROVED		
		SIZE C | DWG NO Final_stage 1 | REV
		SCALE 12 : 1 | SHEET 5 OF 5

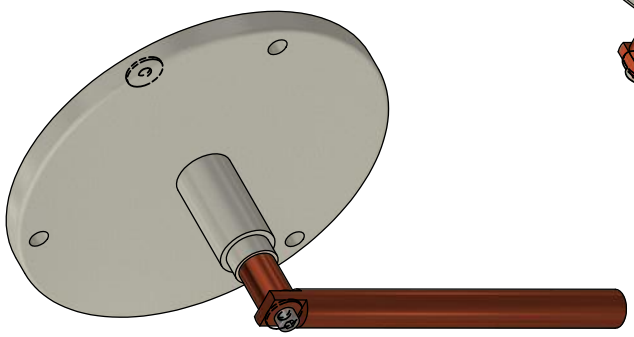

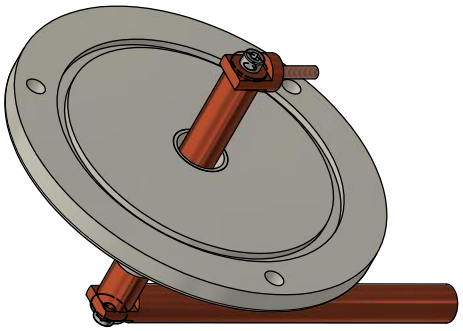

DRAWN bernard Sohl		TITLE	Thermal Feedthrough Flange	REV	
		SIZE D	DWG NO flange full		
		SCALE 1 : 1		SHEET 1 OF 5	

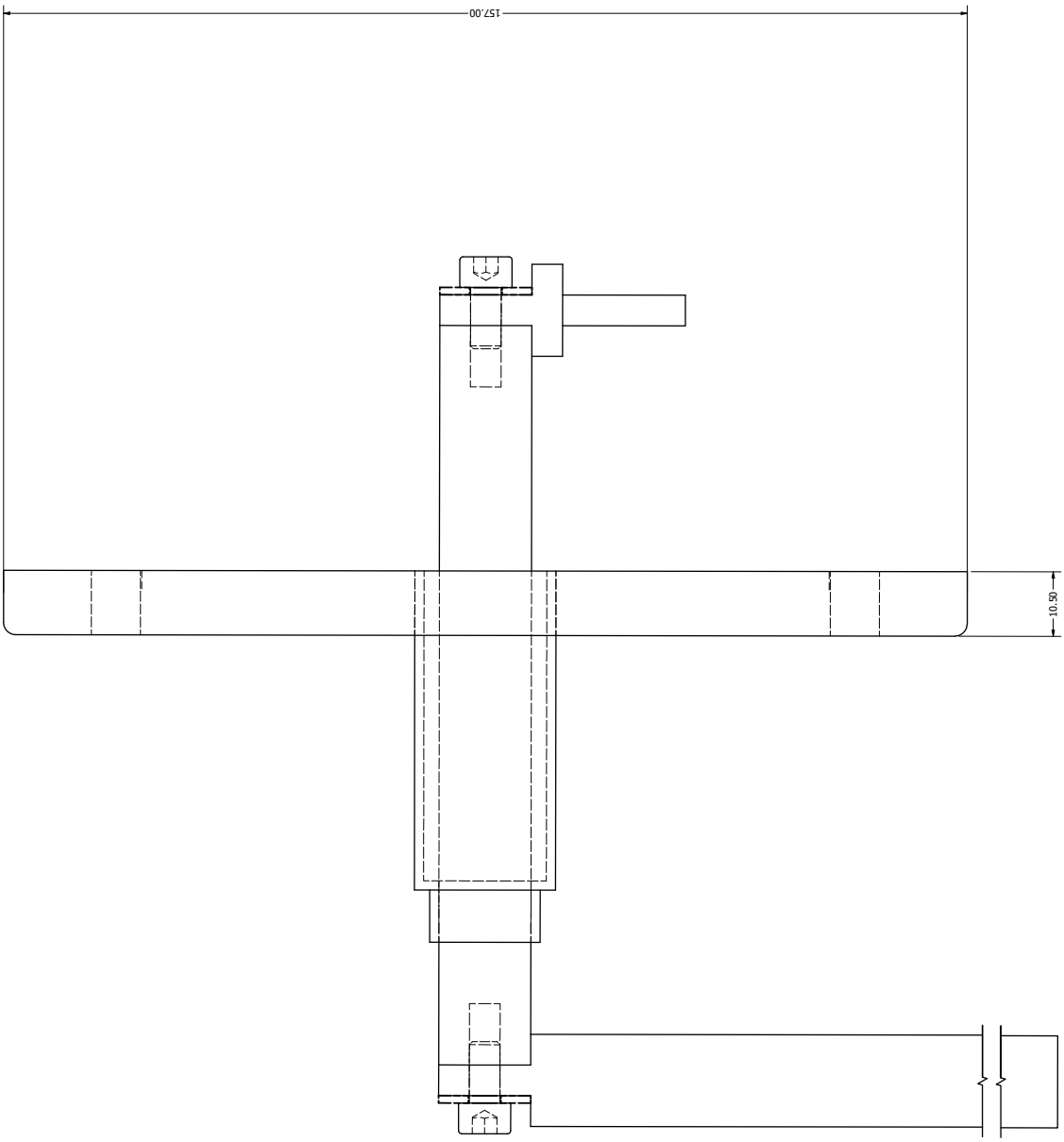

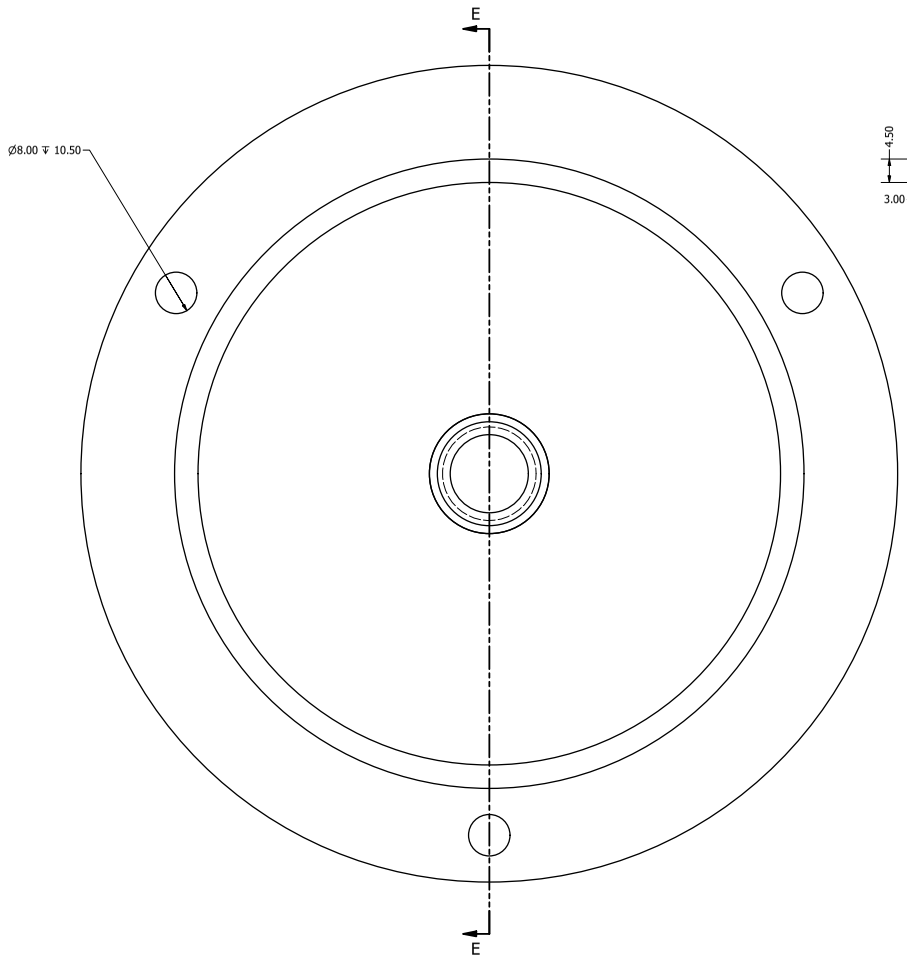

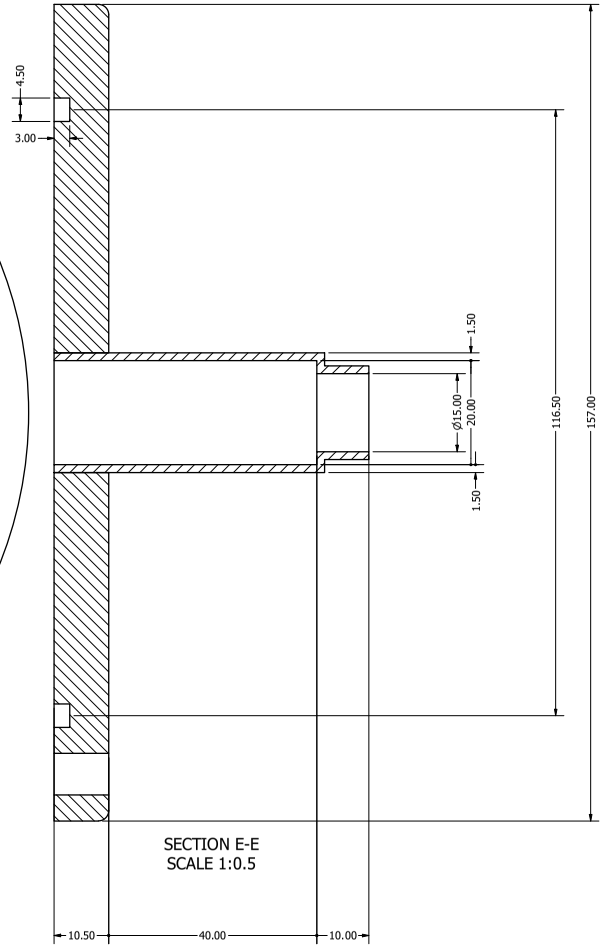

SECTION E-E
SCALE 1:0.5

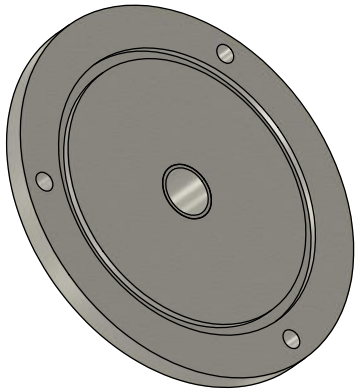

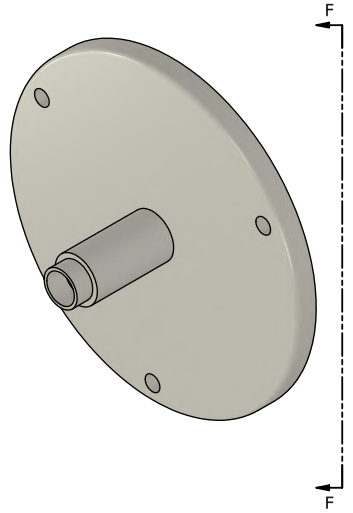

DRAWN	bernard Sohl
TITLE	Thermal Feedthrough Flange
SIZE	D
DWG NO	flange full
REV	
SCALE	1 : 1
SHEET 2 OF 5	

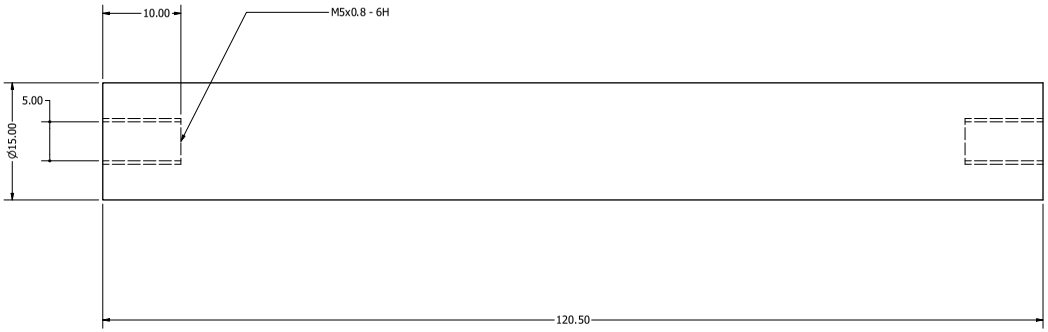

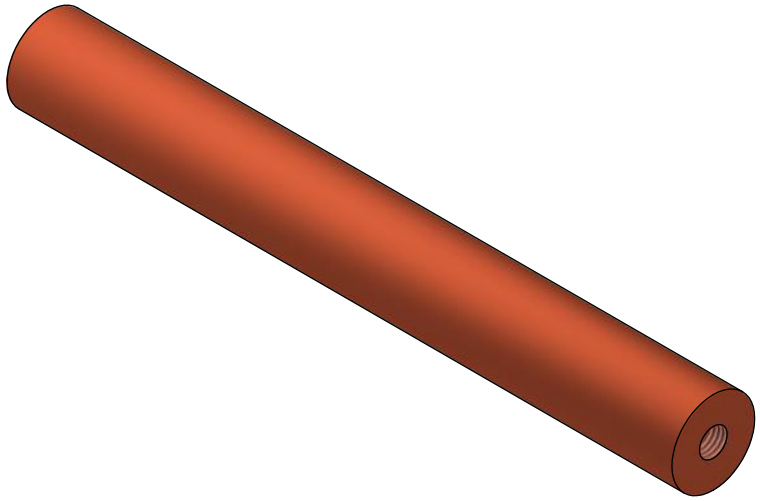

DRAWN	bernard Sohl
TITLE	Thermal Feedthrough Flange
SIZE	D
DWG NO	flange full
REV	
SCALE	3 : 1
SHEET	3 OF 5

DRAWN bernard Sohl		TITLE Thermal Feedthrough Flange		REV
			SIZE D	DWG NO flange full
			SCALE 2 : 1	SHEET 4 OF 5

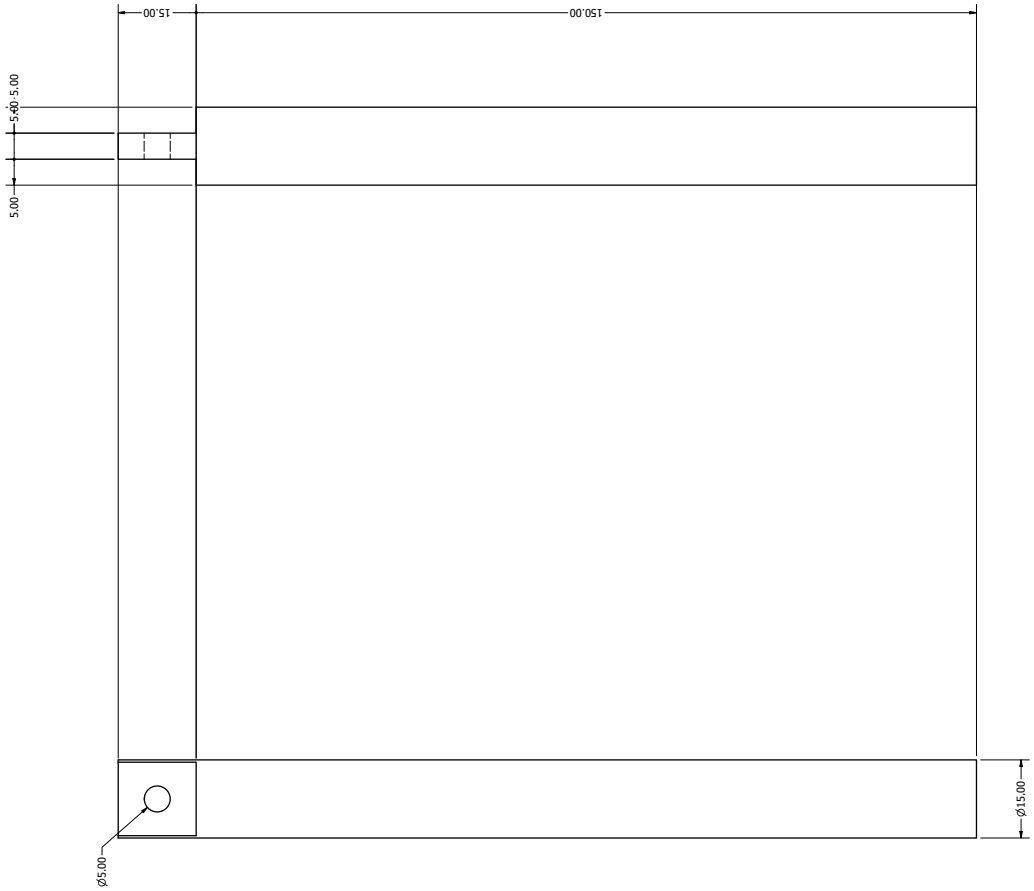

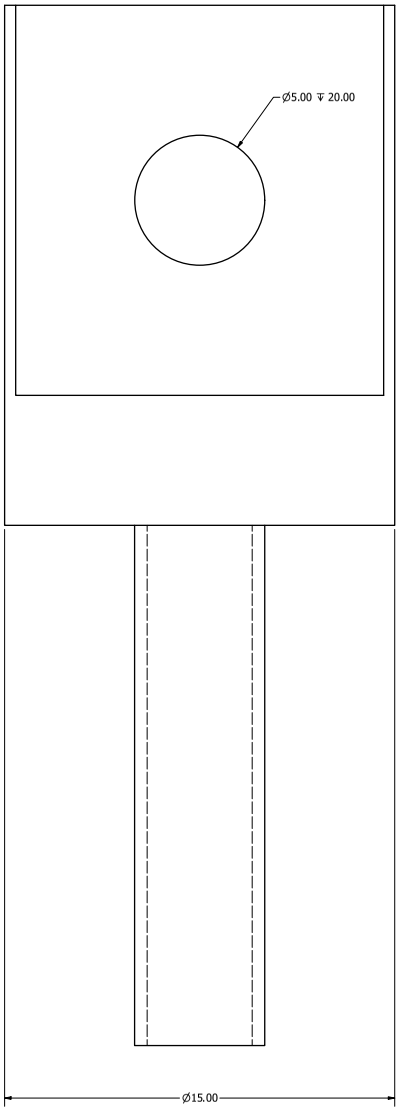

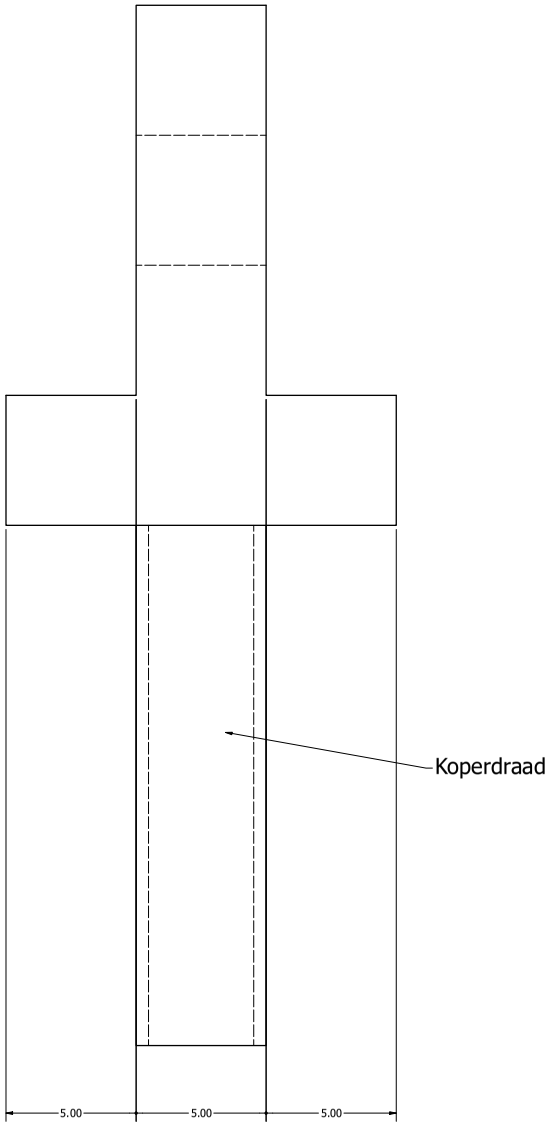

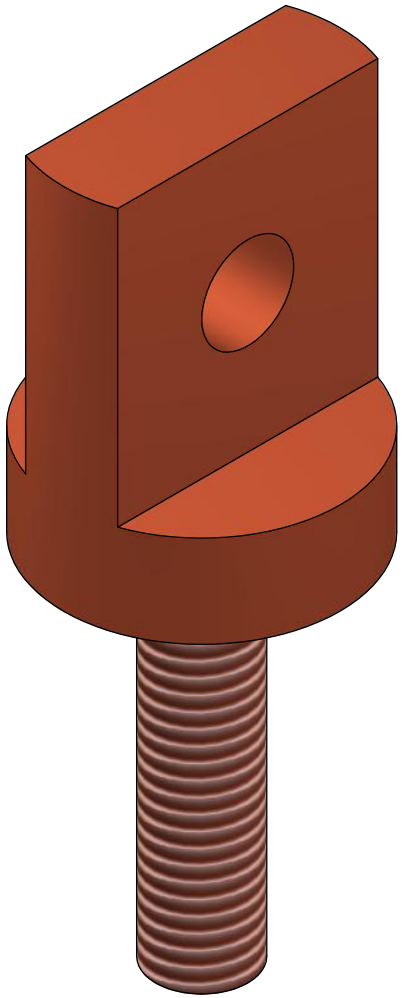

DRAWN bernard Sohl		
		TITLE: Thermal Feedthrough Flange
		SIZE: D · DWG NO: flange full · REV:
		SCALE: 10 : 1 · SHEET 5 OF 5

Bibliography

[ele]

[2] (2022).

[3] Berg, J. (2021). MinimalModbus.

[4] Blom, T., Mechielsen, T., Fermin, R., Hesselberth, M., Aarts, J., and Lahabi, K. (2020). Direct-write printing of josephson junctions in a scanning electron microscope. *ACS Nano*, 15:322–329.

[5] Bresin, M., Toth, M., and Dunn, K. A. (2012). Direct-write 3d nanolithography at cryogenic temperatures. *Nanotechnology*, 24(3):035301.

[6] Bret, T., Mauron, S., Utke, I., and Hoffmann, P. (2005). Characterization of focused electron beam induced carbon deposits from organic precursors. *Microelectronic Engineering*, 78:300–306.

[7] Byeong Seon, A., Kwon, Y., Oh, J.-S., Shin, Y.-J., Ju, J.-s., and Yang, c.-W. (2019). Evaluation of ion/electron beam induced deposition for electrical connection using a modern focused ion beam system. *Applied Microscopy*, 49.

[8] Edinger, K., Becht, H., Bihr, J., Boegli, V., Budach, M., Hofmann, T., Koops, H. W. P., Kuschnerus, P., Oster, J., Spies, P., and Weyrauch, B. (2004). Electron-beam-based photomask repair. *Journal of Vacuum Science Technology B: Microelectronics and Nanometer Structures Processing, Measurement, and Phenomena*, 22(6):2902–2906.

[El-Dardiry] El-Dardiry, R. Leidenfrosteffect: Zwevende druppels. *Natuurkunde.nl*.

[10] Ellis, G. (2012). Chapter 6 - four types of controllers. In Ellis, G., editor, *Control System Design Guide (Fourth Edition)*, page 111. Butterworth-Heinemann, Boston, fourth edition edition.

[11] Haque, R. I., Waafi, A. K., Jaemin, K., Briand, D., and Han, A. (2022). 80 k cryogenic stage for ice lithography. *Micro and Nano Engineering*, 14:100101.

[12] Kohlmannâvon Platen, K. T., Buchmann, L., Petzold, H., and BrÃŒnger, W. H. (1992). Electronâbeam induced tungsten deposition: Growth rate enhancement and applications in microelectronics. *Journal of Vacuum Science Technology B: Microelectronics and Nanometer Structures Processing, Measurement, and Phenomena*, 10(6):2690–2694.

[13] Mulders, J. J. L., Belova, L. M., and Riazanova, A. (2010). Electron beam induced deposition at elevated temperatures: compositional changes and purity improvement. *Nanotechnology*, 22(5):055302.

[14] OrÃºs, P., Sigloch, F., Sangiao, S., and De Teresa, J. M. (2021). Cryo-focused ion beam-induced deposition of tungstenâcarbon nanostructures using a thermoelectric plate. *Applied Sciences*, 11(21).

[15] Postek, M., VladÃ¡r, A., and Kavuri, P. (2014). Does your sem really tell the truth? how would you know? part 2. *Scanning*, 36.

[16] Randolph, S. J., Fowlkes, J. D., and Rack, P. D. (2005). Effects of heat generation during electron-beam-induced deposition of nanostructures. *Journal of Applied Physics*, 97(12):124312.

[17] Silvis-Cividjian, N., Hagen, C. W., Kruit, P., v.d. Stam, M. A. J., and Groen, H. B. (2003). Direct fabrication of nanowires in an electron microscope. *Applied Physics Letters*, 82(20):3514–3516.

[18] Stewart, R. L. (1934). Insulating films formed under electron and ion bombardment. *Phys. Rev.*, 45:488–490.

[19] Utke, I., Bret, T., Laub, D., Buffat, P., Scandella, L., and Hoffmann, P. (2004). Thermal effects during focused electron beam induced deposition of nanocomposite magnetic-cobalt-containing tips. *Microelectronic Engineering*, 73-74:553–558. Micro and Nano Engineering 2003.